Effect of roll damping tanks on the motion of offshore wind turbine platforms

Auteur : Rasheed, Bushra
Promoteur(s) : Rigo, Philippe
Faculté : Faculté des Sciences appliquées
Diplôme : Master : ingénieur civil mécanicien, à finalité spécialisée en "Advanced Ship Design"
Année académique : 2023-2024
URI/URL : http://hdl.handle.net/2268.2/22249

Universität Rostock
Traditio et Innovatio

LIÈGE université

CENTRALE NANTES

POLITÉCNICA

icam

SOLENT UNIVERSITY SOUTHAMPTON

UNIVERSITÀ DEGLI STUDI DI GENOVA

Zachodniopomorski Uniwersytet Technologiczny w Szczecinie

With the support of the Erasmus+ Programme of the European Union

HOPPE

Effect of Roll Damping Tanks on the Motion of Offshore Wind Turbine Platforms

Master of Science Thesis

Submitted on 5th August 2024

by

RASHEED Bushra | Papenmoorweg 22 | 22869, Schenefeld | bushrarashid@live.com

Student ID No.: 223202144

First Reviewer:

Prof. Dr.-Ing. Florian Sprenger
Professor, Chair of Ship Design
University of Rostock
Albert-Einstein str.2
18059, Rostock
Germany

Second Reviewer:

M.Sc. Aaqib Khan
Project Leader
Hoppe Marine GmbH
Kieler str. 318
22525, Hamburg
Germany

EMship+ Advanced Design

Master's Thesis
University of Rostock

TABLE OF CONTENTS

ABSTRACT

Roll Damping Tanks (RDTs) are passive roll-damping devices, employed in vessels to minimize roll motion. However, their efficacy in controlling the motion of floating offshore platforms has not been widely researched. This thesis investigates the effect of roll damping tanks on the motion response of an offshore wind turbine platform. It further analyzes whether roll-damping tanks are beneficial for a selected semi-submersible platform design. A semi-submersible Floating Offshore Wind Turbine (FOWT) platform, "SEAWORTHY" from Floating Power Plants (FPP) is selected for tank integration.

Design evaluation of the RDT system for the selected platform is conducted using in-house methodologies developed at Hoppe Marine. A C-shaped box tank is designed and its placement within the General Arrangement (GA) of the platform is determined. Computational Fluid Dynamics (CFD) analysis is conducted using OpenFOAM to obtain moment-phase diagrams with respect to motion of the designed tank. A methodology for open-source CFD analysis of RDTs on clusters is developed. Benchmark studies using experimental data from Field & Martin and HERMes roll damping tanks are performed to validate the proposed CFD set-up and methodology. After validation of previous benchmarks, a parameterized model of the designed C-shaped tank is developed and analyzed. The resultant moment-phase curves are calculated for the designed tank and converted into added mass and damping coefficients for the platform.

Finally, a sea-keeping analysis using the open-source tool NEMOH is performed to compare two configurations of the FOWT platform: with and without the RDT integrated. For benchmarking, the roll Response Amplitude Operator (RAO) of the platform without tank is compared with the RAO provided by FPP. Subsequently, the roll damping provided by the tank is incorporated into the platform's RAO. The effect of variation in the mass distribution and the stiffness of the platform due to tank integration is investigated and the modified RAO is computed. The influence of viscous damping is also studied. Final conclusions are drawn by calculating the percentage reduction in peak of roll RAO, highlighting the designed RDT's effectiveness for motion control. It was concluded that the platform's high initial viscous damping significantly limits the tank's roll damping effectiveness. The efficacy of RDT is also reduced by increase in Vertical Center of Gravity (VCG) of platform after tank integration.

DECLARATION OF AUTHORSHIP

I, Bushra Rasheed, declare that this thesis and the work presented in it is my own and have been generated by me as a result of my own original research.

Where I have consulted the published work of others, this is always clearly attributed.

Where I have quoted from the work of others, the source is always given.

With the exception of such quotations, this thesis is entirely my own work.

I have acknowledged all main sources of help.

Where the thesis is based on work done by myself jointly with others, I have made clear exactly what was done by others and what I have contributed myself.

This thesis contains no material that has been submitted previously, in whole or in part, for the award of any other academic degree or diploma.

I cede copyright of the thesis in favour of the University of Rostock, Hoppe Marine GmbH and Floating Power Plants (FPP).

Date & Location:

04-08-2024, Hamburg

Germany

Signature

ACKNOWLEDGEMENTS

I would like to express my deepest gratitude to my company advisors, Mr. Aaqib Gulzar Khan & Mr. Christian Voosen and university supervisor Dr.-Ing. Florian Sprenger for their continuous mentorship throughout my thesis. I am also grateful to Mr. Junheng Zhang, who provided his constructive feedback on all technical and conceptual problems I faced during my analysis. I would like to acknowledge the support of my colleagues at Hoppe Marine, especially Ms. Mona Wilhelm, Mr. Neil Alex, Mr. Imadudin Syaefil Aziz for their help in understanding the company's practices regarding design & analysis of RDTs and others for their moral support. I also extend my gratitude towards Mr. Pablo Cena Martinez and Mr. Lander Galera from Floating Power Plants (FPP) for helping me acquire the data for platform sea-keeping analysis.

Special thanks to my friend and EMShip+ classmate from ECN, Mr. Smit Dhanani, who guided me about the use of NEMOH and helped shape the direction of my thesis. I am particularly thankful to my EMShip+ classmate Mr. Abhemanyu Palaniswamy for his reliable academic insights over the course of EMShip+. I'm also grateful to my friend at URO, Mr. Jay Darji for his help in understanding mesh generator tool Gmsh. In addition, I would like to acknowledge my EMShip+ Alumni who offered me valuable advice on choosing the thesis topic and assistance with thesis writing formats.

I am deeply grateful to Dr.-Ing. Thomas Lindemann for his administrative support, Prof. Philippe Rigo for giving me an opportunity to be part of this program and to all my professors at URO and uLiege for providing me strong academic background in my degree.

My heartfelt thanks go to my family for their encouragement throughout this journey. Specifically, to my mother, Yasmeen Tahira, whose dedication ensured that her daughters received the highest quality education. To my friends Febin, Arum, Karina, thank you for your unwavering support throughout this program.

LIST OF FIGURES

LIST OF TABLES

ABBREVIATIONS

AMP_T	Amplification factor of tank
BMT	Bench Model Test
CFD	Computational Fluid Dynamics
CFL	Courant–Friedrichs–Lewy
CoG	Centre of Gravity
CoR	Center of Rotation
DoF	Degree of Freedom
FFT	Fast Fourier Transform
FOWT	Floating Offshore Wind Turbine
FPP	Floating Power Plants (company name)
FSM_T	Free Surface Moment of tank
MTLD-FB	Multiple -Tuned Liquid Damper with a Floating Base
RANS	Reynold-Averaged Navier-Stokes
RAO	Response Amplitude Operator
RDT	Roll Damping Tank
SDA	Ship Design Analysis
TLCD	Tuned Liquid Column Damper
TLC-BD	Tuned Liquid Column Ball Damper
TLD-FB	Tuned Liquid Damper with a Floating Base
TLP	Tension-Leg Platform
VCG	Vertical Centre of Gravity
VoF	Volume of Fluid
WTG	Wind Turbine Generator

NOMENCLATURE

Symbol	Meaning	Unit
φ	Roll angle	[rad] / °
t	Time	[s]
M_{add44}	Added mass moment of inertia for roll	[kg-m^2]
M_{44}	Mass moment of inertia for roll	[kg-m^2]
B_{44}	Roll damping coefficient	[N-m-s]
K_{44}	Transverse restoring/stiffness coefficient	[N-m]
F_E	Wave excitation moment	[N-m]
φ_a	Maximum roll amplitude	[rad] / °
ω	Roll frequency	[rad/s]
I_{xx}, I_{yy}, I_{zz}	Principle mass moment of Inertia	[kg-m^2]
I_{xy}, I_{yz}, I_{zx} , I_{yx}, I_{zy}, I_{xz}	Product of inertia	[kg-m^2]
I_{xx}	Second moment of area	[m^4]
ρ	Density	[kg/m^3]
A	Waterplane Area	[m^2]
V	Displacement	[m^3]
GM_T	Transverse Metacentric Height	[m]
GM_L	Longitudinal Metacentric Height	[m]
Δ	Displacement	[tons]
$X(\omega)$	Generalized six degrees of freedom response of platform	[m] / [rad]
α	Angular acceleration	[rad/s^2]
h_f	Water level in tank	[m]
B_T	Tank width	[m]
C_T	Tank frequency coefficient	-
K_M	Mooring stiffness coefficient	[N-m]
M_{tare}	Tare Moment	k.N/deg
θ	Roll angle of input motion for BMT	[rad]
θ_o	Maximum amplitude of the input motion for BMT	[rad]
M_R	Resultant Moment	k.N/deg

i	Second moment of area of tank	m^4
ε	Phase difference	[rad]
u_{xi}	Velocity vector in ith mesh volume in x-direction	[m/s]
x_i	Characteristic mesh size of ith mesh volume in x-direction	[m]
Δt	Time step	[s]
λ	Scale factor	-
KB	Distance between keel and center of buoyancy	[m]
BM	Metacentric radius	[m]
KG	Distance between keel and center of gravity	[m]

1 INTRODUCTION

Offshore wind energy has gained traction as a viable alternative to traditional fossil fuel-based power for renewable energy generation. It harnesses the vast energy potential of oceans to produce clean and sustainable power. However, the harsh marine environment poses significant challenges to the efficient operation and structural integrity of the offshore wind turbine platforms. Uncontrolled motions can present significant challenges to the various maritime operations and activities. In the cruise industry, excessive vessel movements can disrupt recreational activities and compromise passenger comfort levels. For container ships, a substantial portion of the cargo is typically stored on exposed decks, subjecting it to significant accelerations induced by rolling motions. Such conditions can lead to internal damage to the containerized goods, and in extreme cases, result in the failure of securing mechanisms, potentially causing containers to be lost overboard.

In the offshore industry, the platform motions induced by the wave and wind forces can adversely impact the performance and longevity of wind turbines. Excessive motions due to wave loads also impede precise maintenance operations. Marine operations, such as maintenance, inspection, and crew transfer, require minimal platform motions for safe and effective execution. Controlling roll and pitch motions is therefore essential for ensuring the precision and safety of these engineering tasks. In addition, uncontrolled roll responses can also have a negative impact on mooring systems. To mitigate this issue, various motion control devices have been developed, including tuned liquid dampers for wind turbine tower vibrations. However, the use of roll damping tanks specifically for enhancing the dynamic stability of offshore platforms against wave forces is still not widely researched and employed commercially.

1.1 Executive Summary

This thesis investigates the impact of roll damping tanks on the motion of offshore wind turbine platforms, exploring their designs, configuration, and impact on the platform dynamics. The study encompasses a comprehensive investigation into the design of RDT for a T-shaped semi-submersible floating offshore wind turbine (FOWT) platform from the company Floating Power Plants (FPP). Computational Fluid Dynamics (CFD) simulations are performed to compute moment-phase curves for different frequencies using OpenFOAM. For the validation of CFD analysis with Reynolds-Averaged Navier-Stokes (RANS) turbulence modelling, two benchmark studies on Field & Martin and HERMes tank are conducted. Lastly, sea keeping analysis, which involves studying the motion response of floating structures in waves, is conducted for the platform with and without roll damping tanks, utilizing tools such as NEMOH. In the end, the effect of the roll damping tank to reduce roll motion of the platform is analyzed in regular waves.

1.2 Roll Damping Tanks (RDTs)

Roll motion of a vessel is considered one of the most critical motions, as the transverse moment of inertia for vessels is very small compared to the longitudinal one, leading to increased chances of capsizing on excessive roll. To control this roll motion, various roll damping devices are employed in a vessel, which can be divided into active and passive roll damping devices. Active stabilization systems require energy input and can adapt to changing wave conditions. These include rudder stabilizers, active fins or gyro stabilizers. Passive roll damping devices include roll damping tanks and bilge keels. RDTs create a moment out of phase to ship's roll motion without the need of active energy input, while bilge keels reduce roll by dissipation of kinetic energy through vortex formation. However, bilge keels require the ship to move to provide roll damping while roll damping tanks provide damping even when the vessel is not underway. [1]

The Roll Damping Tanks (RDTs) stabilize a vessel by creating a moment which is out of phase to the moment of roll created by waves. This out-of-phase moment is created by tuning the movement of liquid in such a way that it lags a quarter cycle (90°) behind the vessel's roll motion during resonant rolling. At resonance, the phase difference between wave excitation and roll motion approaches 90°. This leads to a total phase lag of 180° between wave excitation and liquid motion in roll damping tanks, thereby stabilizing the vessel by creating moment opposite to waves. While RDTs decrease the roll amplitude of ship at resonance wave excitation frequencies, they can also add to roll increase at frequencies below and above the resonance period due to hydrodynamic added mass effects. Therefore, it is essential to design the tank to achieve a near-to 90° phase shift between the tank and the ship motion at non-resonant frequencies as well. This effect is discussed in detail in Section 1.3.1.

1.3 Types of Tanks

Based on their shapes and working principle, RDTs can be categorized into two types, as discussed below:

1.3.1 Box-Shaped Tanks

Box-shaped tanks are designed with the fluid's free surface extending from the starboard to the port side of the tank. A box-shaped tank, typically called flume tank, is shown in Figure 1-1. These tanks minimize ship roll motion by utilizing the forces generated by the sloshing fluid against the tank walls. The natural period of tank's sloshing motion is tuned to match the natural roll period of the ship, thereby creating anti-resonance at the resonance frequency of the ship's roll motion. This is done by adjusting tank's water level; hence flume tanks can provide damping against several loading conditions by adjusting water level [2]. The tank dimension along x-axis is considered the length of tank, the beam is along y-axis and height is considered along z-axis. For a given tank beam, increasing water level leads to smaller time periods (Hoppe database). Additionally, flooded baffles and internal structures like T-shaped or flat stiffeners and nozzle plates are often installed within the tanks to regulate the damping ratio of the sloshing motion, as shown in Figure 1-1.

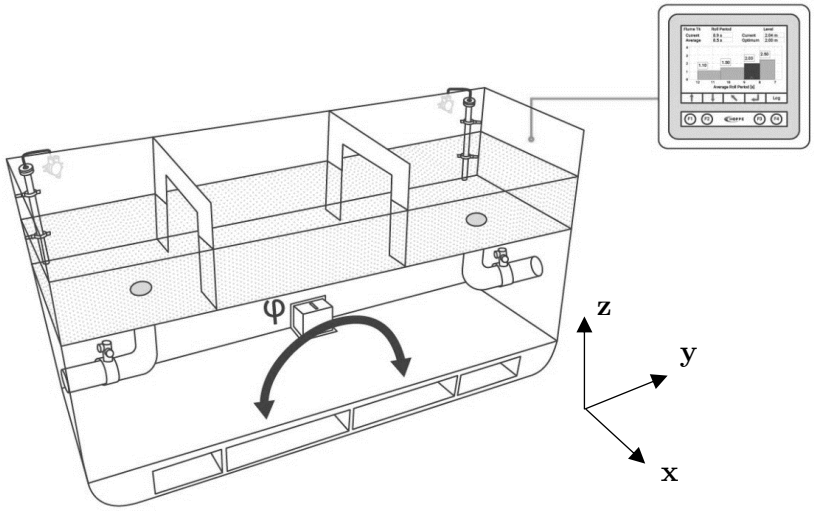

Figure 1-1: Flume tank with nozzle plates [Hoppe Database]

The configuration of these free-surface flume tanks can be adjusted depending on the available space in the general arrangement. Various designs for flume tanks, including C-shaped and I-shaped, are shown in Figure 1-2.

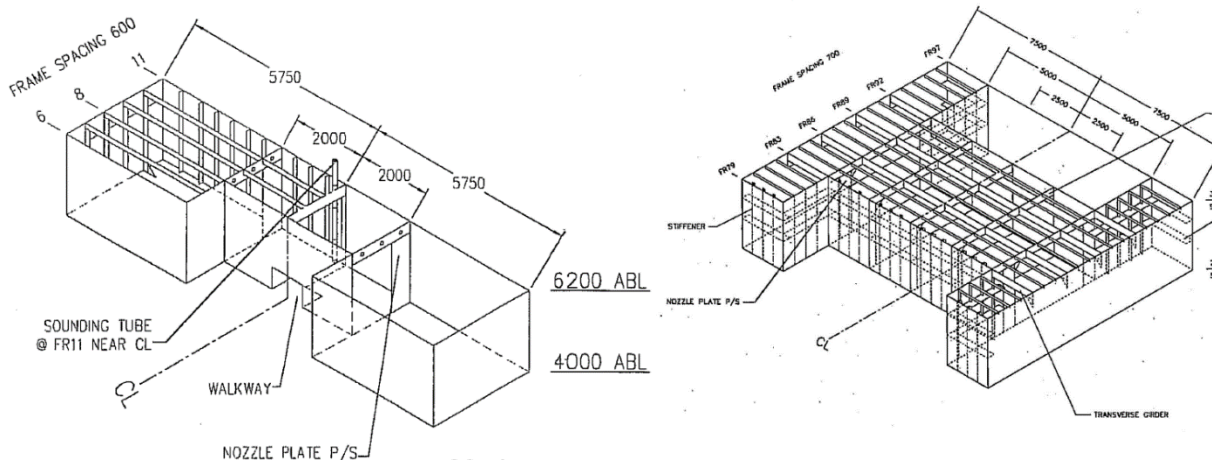

Figure 1-2: Box-shaped tank designs [Hoppe Database]

1.3.2 U-Tanks

These roll damping tanks resemble a U-shape, with two wing tanks on port and starboard side connected by a cross-duct at the bottom. In some modified designs of the U-shaped tanks, several air ducts connect the two wing tanks at the top and provide an active fluid-control with the help of the valves. The time period of liquid movement inside the tank can be controlled by adjusting the area ratio of the free surface in wing tanks and of the cross-duct connecting the two wing tanks. A passive U-tank with air-ducts is shown in Figure 1-3.

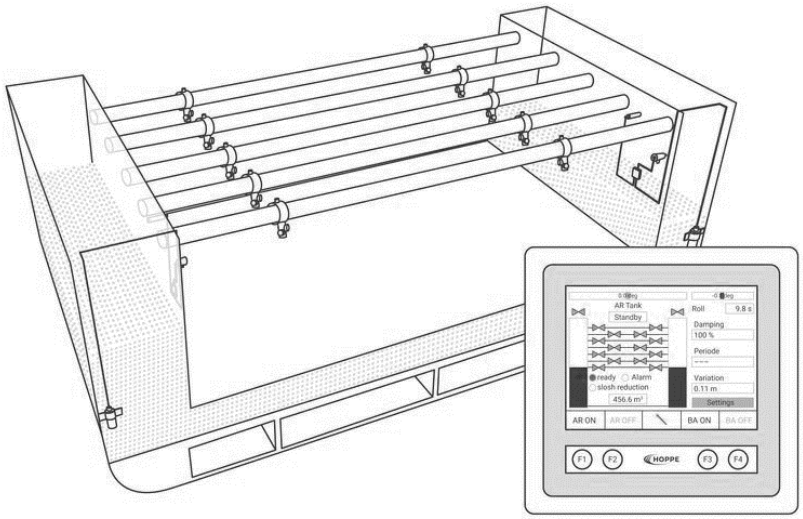

Figure 1-3: Hoppe U-tank with air-ducts [Hoppe Database]

While the free surface box-shaped tanks are entirely passive, U-tanks can be made active by connecting a pump in between the connecting duct that joins two wing tanks. The pump helps transport water from one wing tank to another according to a control command, which leads to a change in the roll period of tank, providing reduced vessel motion around both fundamental and principle parametric resonance. If an efficient control loop is designed for the pump control command, the active RDTs can outperform passive RDTs. This improvement occurs without increasing roll at non-resonant frequencies due to the added mass. RDTs require pumps with variable frequency drives that control the speed and torque of pumps. These pumps fine-tune the liquid motion according to ship roll in real-time. While the usage of active RDTs can lead to roll reduction across a range of sea-states and loading conditions, the concept of such active RDTs is limited to theoretical and experimental studies only. This is because active RDTs are more complex, and require sensors, control systems and power source to operate. This can lead to higher installation and maintenance costs [2] [3].

2 LITERATURE STUDY

Before the advent of floating structures, offshore wind turbines were constrained to fixed platforms, restricting their deployment to the shallow waters. The fixed platforms include monopile, jacket, tripod, and gravity base substructures. However, with the ongoing technological progress, various design models for floating wind turbine platforms have emerged. These include barge, spar, Tension-Leg Platform (TLP) and semi-submersible foundations [4], as shown in Figure 2-1.

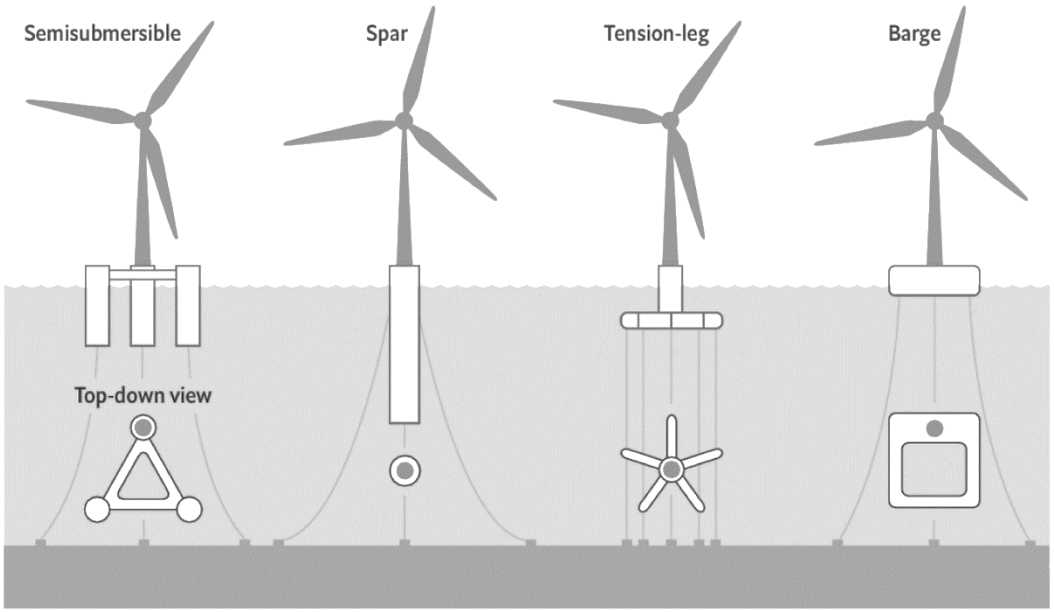

Figure 2-1: Platform design models for FOWTs [4]

Out of the above-mentioned design models, the semi-submersible platforms are gaining an increased traction for Floating Offshore Wind-Turbines (FOWTs), as they offer several advantages. One of their prominent advantages is that they eliminate the need for towing and installation equipment during the installation process, unlike fixed platforms. Additionally, they provide more deck space for maintenance and are not constrained by a minimum water depth requirement for installation. Furthermore, they have a proven technology for FOWTs, with over 70 MW of cumulative installed capacity across various floating wind projects that have selected this foundation design. Compared to semi-submersibles, other design models like TLP and Spar either have low technology readiness level for FOWTs or their installation capacity is low and are not properly commercialized yet [5].

One drawback of floating offshore wind turbines is the excessive platform motions due to waves, which can interfere with the maintenance activities, inspection and crew transfer. Platform motion also interferes with the energy yield of FOWTs. When the semi-submersible platform pitches, it induces an average pitch angle in the rotor plane, which effectively reduces the angle of attack of the blades. This in turn leads to a reduction in angle of attack, which results in

less power generation than a fixed-bottom turbine [6]. Platform motions can cause unsteady aerodynamic effects and wake interactions that impact power generation. Liu et al. [7] showed that the superposition of platform motion has significant impact on thrust and torque, leading to potential structural stress and fatigue related problems. The wake interactions between the rotor and the platform can further influence the power output of the turbine, both positively and negatively, depending on the specific motion characteristics.

Various devices have been developed to reduce the excessive motions of floating offshore wind-turbines. One of them is a tuned liquid damper with a floating base. A tuned liquid damper is a device used to control the vibrations induced by the sway motion in structures such as bridges, buildings, wind-turbine towers etc. It consists of a liquid-filled container that moves in response to structure's vibrations, thereby damping the vibration due to inertia of moving liquid. In [8], Chatterjee, T., & Chakraborty, S. present a simple model of a Tuned Liquid Column Damper (TLCD) as shown in Figure 2-2. They showed the efficacy of Tuned Liquid Column Damper (TLCD) and Tuned Liquid Column Ball Damper (TLCBD) as passive vibration control devices for mitigating wave induced vibration of offshore structures.

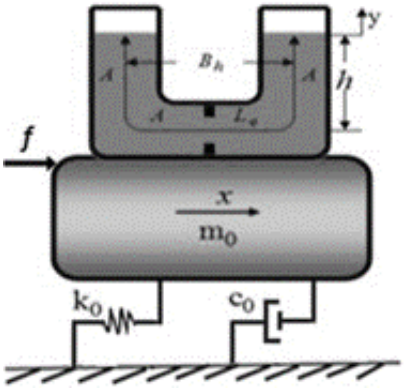

Figure 2-2: Basic design of Tuned Liquid Column Damper (TLCD) [8]

R. Sardar and S. Chakraborty [9] explored the prospect of using a deep-water storage tank as Tuned Liquid Damper with a Floating Base (TLD-FB). To control the vibration of offshore platforms caused due by wave-induced load, they proposed multiple TLD with floating-base (MTLD-FB) as a modification of the TLD-FB for a large water storage tank. The numerical analysis concluded that attaching multiple TLD with a jacket platform significantly controls the wave-induced vibrations in four loading conditions, providing maximum reduction of 24% in displacement and 34% in acceleration.

The use of roll damping tanks to control the excessive motions of vessels is not a new concept. The development of RDT systems began with Froude in 1874, who installed water chambers in ships for stabilization against rolling. Significant progress resumed in 1910 with Frahm's U-tube tank, widely implemented in German shipping industry. Research surged in the 1960s and 1970s, with Vasta et al. [10] reviewing Navy developments and tank design, and Stigter [11] providing foundational equations for U-tube tanks. In 1966, Bell and Walker [12] explored two types of controlled–passive tanks using valves in air duct or water channel. In 1967, Webster analyzed pump-activated U-tube tanks and demonstrated the optimization of roll tank by minimizing the ship response against an impulsive roll [13]. Field and Martin's [14] study

compared U-tube and free-surface tanks experimentally, while Lewison [15] optimized free-surface tank design mathematically. Barr and Ankudinov [16] provided a critical review of predictive methods for roll reduction. In 1988, Webster et al. [17] investigated free-flooding tanks concept on the upgrade of USS Midway. Study by Lee and Vassalos [18] focused on the effect of internal flow obstructions in roll damping tanks. Significant efforts have addressed nonlinear rolling motions in various sea conditions, with contributions from researchers like Nayfeh and Falzarano [19].

However, the use of roll damping tanks for floating offshore structures and its feasibility study has low technology readiness levels, with only few studies focusing on the effect of roll damping tanks for offshore wind turbine platforms. One such study was performed by Borg, M. et al. [20] which aimed at analyzing the motion reduction provided by different passive damping devices, including open-bottom tanks (for heave), heave bottom plates and roll damping tanks. In this study, the motion reduction provided by U-shaped anti-roll tank designed for a tri-floater offshore platform design was calculated to be around 2% only, while the open bottom tanks provided roll reduction of around 20.6%. A thorough study of this investigation points out that a tank of width 9 m was used in the design stage, while the length between columns of tri-floater used in the study is 52 m. This alters the free surface moment calculation by a factor of twenty, hence explaining why a reduction of 2% was obtained instead of 20-40%.

Another similar study was performed by Franzel [21] for Ideol's floating offshore wind turbine platform SQUATINA and offshore substation, the optiFloat project. A U-shaped anti-roll tank was designed for a barge-shaped offshore wind-turbine platform and its performance in regular and irregular waves was compared with the platform with skirt system for motion reduction. For extreme cases, the study concluded a maximum decrease in the standard deviation of around 30% for a two-tank system, compared to 44% reduction provided by skirt system. It was found in the investigation that optiFloat substation gave maximum decrease in standard deviation of 40% in harmonic oscillation tests while a reduction of only 4% in irregular wave tests. It was revealed in the investigation that optiFloat substation already had high initial damping, which made the employment of roll damping tanks redundant.

To investigate the effect of roll damping tanks on the motion of a platform, different modules of semi-submersible wind turbine platforms, both in commercial and demo stage were studied in this thesis. The current projects by different companies include V-shaped Fukushima Shimpuu 7 MW three column module [22], 8.4 MW WindFloat Atlantic platform by Principle Power [23], 11 MW VolturnUS platform [24] by DeepCWind (company by University of Maine), 9.5 MW pilot project of Groix & Belle-Ile Design by EOLFI [25] and Floating Power Plant's (FPP) SEAWORTHY platform [26] that integrates 4.3 MW wind turbine generator along with wave converters and hydrogen systems. Other platform designs are still in model test/design completion stage and are not demonstrated yet. These include T shaped Bassoe 15MW platform by Bassoe Technology [27], Gusto MSC tri-floater 15 MW design [28] and DeltaFloat design by SOIC accommodating 12 MW wind turbine [29]. The various designs are shown in Figure 2-3. For the implementation of roll damping tank for motion control, the semi-submerisible platform design SEAWORTHY from Floating Power Plants (FPP) was selected.

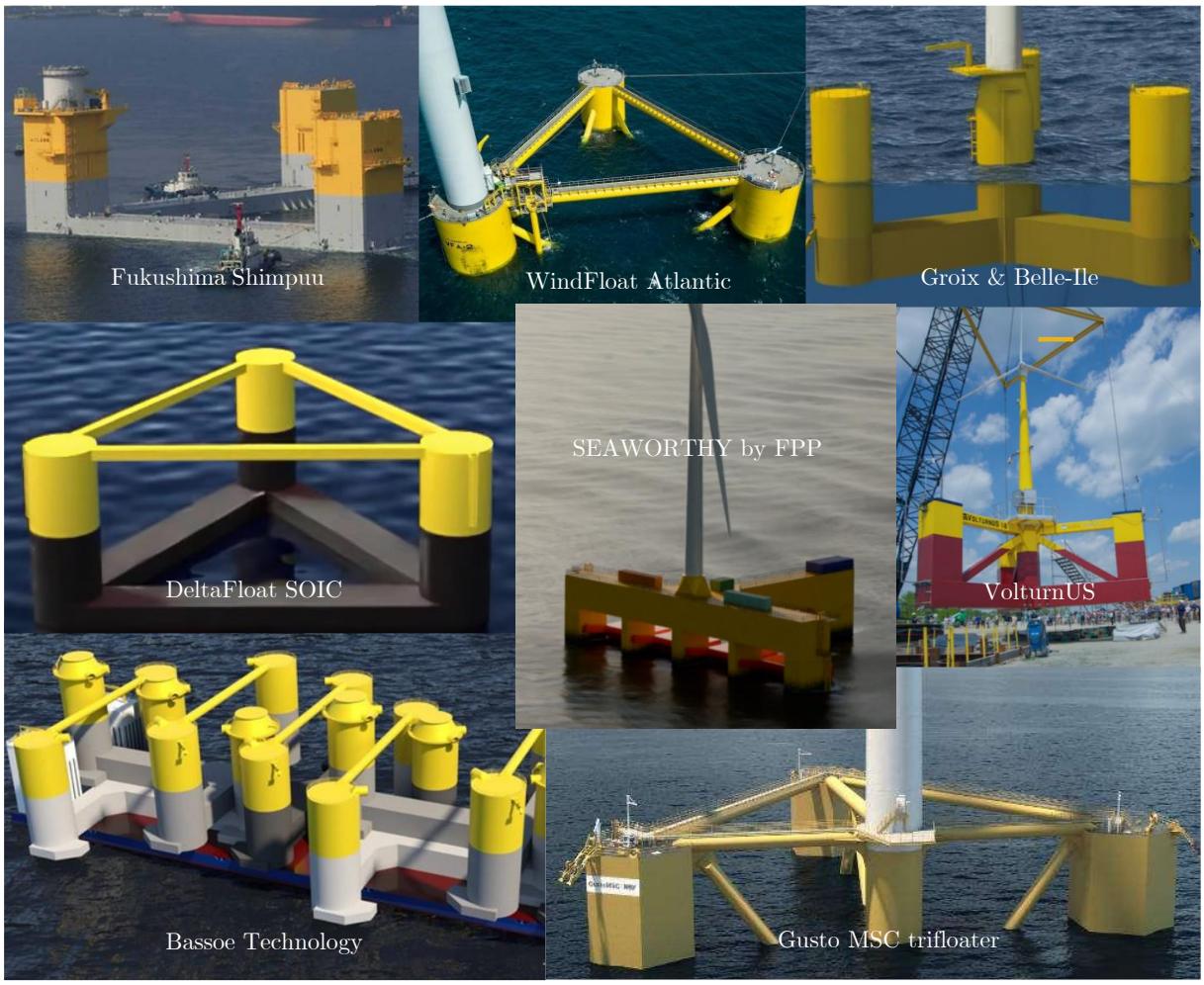

Figure 2-3: FOWT semi-submersible platform designs

The main reason behind the selection was the T-shape of platform, which allows the tank's roll axis to be oriented parallel to the platform's roll axis. This orientation enables maximum roll damping moment transfer from the sloshing liquid to the platform. It also makes it easier to integrate the tank moment in NEMOH, compared to tanks placed at an angle with roll axis.

2.1 Motivation and Objectives

Passive roll damping tanks have been extensively used to manage roll motion in vessels; however, they have not yet been designed or implemented for motion control in offshore semi-submersible platforms. Semi-submersible platform, as opposed to the Tension-Leg Platform or monopiles, experience greater motions, which can hinder maintenance, inspection, and crew transfer onto the platform. Excessive motion can also lead to fatigue-loads in wind turbine and has the potential to affect its energy yield as well. The absence of sufficient research on RDTs for semi-submersible platform motion control is the prime motivation for current thesis. Moreover, a parametrized model of designed tank is required for several design iterations required for tank dimensions. To achieve this, Computational Fluid Dynamics (CFD) analysis via OpenFOAM has been chosen as the preferred method due to the ease of parameterization and lesser time requirements, compared to the model fabrication in experimental tests. It also offers reduced complexity compared to the bench model tests.

This thesis report aims to answer the following questions:

- Can RDT be designed for a given semi-submersible platform, with its roll period matching with eigen period of platform?
- Can CFD analysis in OpenFOAM generate moment-phase diagrams for Roll Damping Tanks (RDTs) that closely align with the experimental bench model tests, while also reducing the time required for analysis?
- How can a methodology be developed that enables the parametrization of tank geometry and automates the computation of RDT at various roll amplitudes & frequency combinations, exclusively using open-source tools?
- Can NEMOH be used to apply damping effect of tank at each frequency in roll RAO of platform?
- What is the effect on roll RAO of platform, once the RDT mass and altered stiffness due to tank, is accommodated in platform?
- How much roll reduction in RAO of un-stabilized platform is achieved, once the tank damping effect is accommodated?
- Are Roll Damping Tanks (RDTs) suitable for controlling roll motion of semi-submersible offshore wind turbine platforms?

3 THEORETICAL BACKGROUND

3.1 Theoretical Background of Roll Damping Tanks (RDTs)

Let us consider a platform without any roll stabilization tank. The equation of motion for an un-stabilized platform in roll can then be written as follows:

$$[M_{44} + M_{add44}]\ \ddot{\varphi}(t) + B_{44}\dot{\varphi}(t) + K_{44}\varphi(t) = F_E(t) \tag{1}$$

Where

φ = roll angle [rad]

M_{add44} = Added mass moment of inertia for roll [kg-m^2]

M_{44}= Mass moment of inertia for roll [kg-m^2]

B_{44}= Damping coefficient [N-m-s]

K_{44} = Transverse restoring coefficient [N-m]

F_E = Wave excitation moment [N-m]

For harmonic motion, roll angle φ and its derivates can be written as:

$$\varphi = \varphi_a\, cos(\omega t) = \varphi_a e^{-i\omega t} \tag{2}$$

$$\dot{\varphi} = -\omega\varphi_a\, sin(\omega t) = -i\omega\ \varphi_a e^{-i\omega t} \tag{3}$$

$$\ddot{\varphi} = -\omega^2\varphi_a\, cos(\omega t) = -w^2\varphi_a e^{-i\omega t} \tag{4}$$

Where

φ_a = Maximum roll amplitude [rad]

ω= Roll frequency [rad/s]

By using linear wave theory, the excitation force will be harmonic and can be expressed as:

$$F_E(t) = F_{E,a}\cos(wt) = \ F_{E,a}e^{-i\omega t} \tag{5}$$

Where $F_{E,a}$ is the amplitude of wave excitation moment.

Equation 1 can be converted in terms of frequency by substituting equation 2, 3 & 4, which leads to the following:

$$-[M_{44} + M_{add44}]\ \omega^2\varphi_a\, cos(\omega t)\ - B_{44}\ \omega\ \varphi_a\, sin(\omega t) + K_{44}\varphi_a\, cos(\omega t) = F_E(t) \tag{6}$$

$$-[M_{44} + M_{add44}]\ \omega^2\varphi - i\omega\ B_{44}\ \varphi + K_{44}\varphi = F_E \tag{7}$$

The moment imparted by roll damping tanks is translated as hydrodynamic added mass and additional damping coefficients. The tank moment is out of phase with roll moment of the ship. Considering that the translation surge, sway and heave are represented by indices 1, 2 & 3 while indices 4,5,6 represent roll, pitch and yaw rotation correspondingly, the equation of motion is then modified as follows:

$$-[M_{44} + M_{add44} + A_{tank44}]\omega^2\varphi - i\omega\,[B_{44} + B_{tank44}]\,\varphi + [K_{44} + K_{tank44}]\varphi = F_E \qquad (8)$$

Where A_{tank44}, B_{tank44} and K_{tank44} are the corresponding added mass, damping coefficient and restoring coefficient added by the tank. Due to addition of mass and increase or decrease in GM (based on location of tank), restoring coefficient and draft will also change consequently.

The above equation of motion can be extended to six degrees of freedom and written in the matrix form as shown in the subsequent section. The mass matrix M, about a point offset from center of gravity point, is given as [30]:

$$M = \begin{bmatrix} m & 0 & 0 & 0 & zm & -ym \\ 0 & m & 0 & -zm & 0 & xm \\ 0 & 0 & m & ym & -xm & 0 \\ 0 & -zm & ym & I_{xx} + m(y^2+z^2) & I_{xy} - mxy & I_{xz} - mxz \\ zm & 0 & -xm & I_{xy} - mxy & I_{yy} + m(x^2+z^2) & I_{yz} - myz \\ -ym & xm & 0 & I_{xz} - mxz & I_{yz} - myz & I_{zz} + m(x^2+y^2) \end{bmatrix}$$

Where,

m =mass of platform

$x,\ y\ ,z$ = Offsets from center of gravity

$I_{xx},\ I_{yy},\ I_{zz}$ = Principle mass moment of inertia

$I_{xy},\ I_{yz},\ I_{zx}\ ,\ I_{yx},\ I_{zy},\ I_{xz}$ = Product of inertia

The second and third quadrants of above matrix contain the first moments produced due to the translation of reference point with offset x, y and z from center of gravity. The added mass matrix is given as follows [31]:

$$M_{add} = \begin{bmatrix} M_{11} & M_{12} & M_{13} & M_{14} & M_{15} & M_{16} \\ M_{21} & M_{22} & M_{23} & M_{24} & M_{25} & M_{26} \\ M_{31} & M_{32} & M_{33} & M_{34} & M_{35} & M_{36} \\ M_{41} & M_{42} & M_{43} & M_{44} & M_{45} & M_{46} \\ M_{51} & M_{52} & M_{53} & M_{54} & M_{55} & M_{56} \\ M_{61} & M_{62} & M_{63} & M_{64} & M_{65} & M_{66} \end{bmatrix}$$

The hydrodynamic linear damping matrix is given by:

$$B = \begin{bmatrix} B_{11} & B_{12} & B_{13} & B_{14} & B_{15} & B_{16} \\ B_{21} & B_{22} & B_{23} & B_{24} & B_{25} & B_{26} \\ B_{31} & B_{32} & B_{33} & B_{34} & B_{35} & B_{36} \\ B_{41} & B_{42} & B_{43} & B_{44} & B_{45} & B_{46} \\ B_{51} & B_{52} & B_{53} & B_{54} & B_{55} & B_{56} \\ B_{61} & B_{62} & B_{63} & B_{64} & B_{65} & B_{66} \end{bmatrix}$$

There is no restoring force produced in surge, sway and yaw so the restoring coefficients are zero for surge, sway and yaw. The stiffness matrix is given as [32][33]:

$$K = \begin{bmatrix} 0 & 0 & 0 & 0 & 0 & 0 \\ 0 & 0 & 0 & 0 & 0 & 0 \\ 0 & 0 & K_{33} & K_{33}y & -K_{33}x & 0 \\ 0 & 0 & K_{33}y & K_{44} & -K_{33}xy & -(\rho gV + mg)x \\ 0 & 0 & -K_{33}x & -K_{33}xy & K_{55} & -(\rho gV + mg)y \\ 0 & 0 & 0 & 0 & 0 & 0 \end{bmatrix}$$

Where *x,y,z* are the coordinates of reference point from center of gravity. The above matrix assumes that center of gravity and center of buoyancy are vertically aligned. Given that A is waterplane area of platform, m is mass, V is displacement in m^3, GM_T is transverse metacentric height while GM_L is longitudinal metacentric height, the expressions for hydrostatic coefficients are given as:

$$K_{33} = \rho g A \tag{9}$$

$$K_{44} = \rho g V G M_T + \rho g A \; y^2 \tag{10}$$

$$K_{55} = \rho g V G M_L + \rho g A \; x^2 \tag{11}$$

The Response Amplitude Operators (RAO) in six degrees of freedom (DoF) are then calculated by solving the following equation of motion*:*

$$\{-[M + M_{add}(\omega)]\omega^2 - i\omega[\, B(\omega) + B_{add}] + [K_h + K_M]\}\; X(\omega) = F_E(\omega) \tag{12}$$

Where $X\ (\omega)$ is the six degrees of freedom response of platform in surge, sway, heave, roll, pitch and yaw. K_h is hydrostatic stiffness coefficient while K_M is mooring stiffness. B_{add} is any additional damping provided either by viscous damping or roll damping tanks.

3.2 Theoretical Background of Bench Model Tests (BMTs)

Bench model test is conducted to calculate the moment and phase diagram of each tank design, thereby validating if the tank design is providing sufficient roll reduction at required phase difference or not. In the test, a Steward platform in the experimental bench, commercially called hexapod, is used to provide six DoF motion to the tank. The distance between center of rotation (CoR) of Stewart platform and center of gravity (CoG) of tank is equal to the distance between center of gravity (CoG) of tank and vertical CoG of ship (VCG). In the test, it is assumed that ship/ platform rotates about its center of gravity.

Tests are carried out at roll amplitudes of 2 °, 5 °, 10° and a range of frequencies corresponding to the expected sea spectrum of the vessel route. The frequency ranges also change according to the loading and operating conditions of the ship, against which roll damping is desired. Before carrying out the test, a motion file is generated comprising of hexapod motion coordinates for all frequencies. The test for all frequencies is carried out together. During the test, around 10 time periods are recorded for each frequency. The bench model test set-up on hexapod is shown in Figure 3-1.

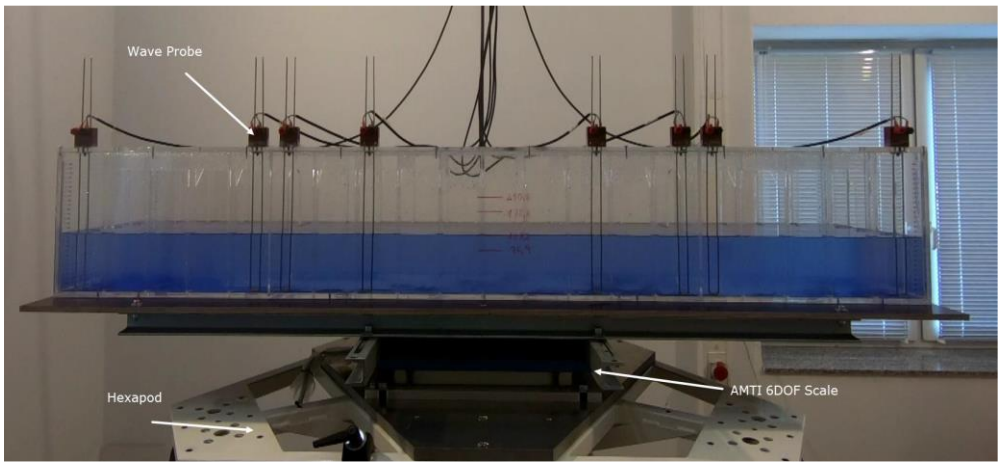

Figure 3-1: Bench Model Test Set-up

For RAO calculations, the data from model tests need to be converted from time domain to frequency domain via Fast Fourier Transform (FFT). **`Filtfilt`** filtering function [34], which is a zero-phase distortion filter in MATLAB, is used to filter and smoothen the time domain data from BMT. However, the results contain transition periods from one frequency to another, which need to be cut out. In MATLAB post-processing, the transition ramp in time domain is clipped out and the signal is sliced before Fourier transformation. Each sliced signal is then transformed into frequency domain using FFT and the result for all sliced signals is averaged.

The total moment of tank contains two parts, the moment generated by flowing water, called resultant moment and the other with water "being frozen", called the tare moment. Tare moment does not participate in producing the damping effect. The difference between total moment and tare moment of the tank gives resultant moment, which shows the influence of free surface on roll damping.

One of the important parameters in bench model tests is the lever arm, which is measured from the bottom of tank to center of rotation of ship/platform. It is positive when the tank's bottom is below ship's CoG and negative when tank's bottom is above ship's CoG.

Tare moment [N-m] can be calculated analytically, as follows:

$$\theta = \theta_o \sin(\omega t) \tag{13}$$

$$\alpha = -\omega^2 \theta \tag{14}$$

$$M_{tare} = -\{\alpha(I_{xx} + m(l-z)^2) + mg(l-z)\theta\} \tag{15}$$

Where,

θ_o = Maximum amplitude of the input motion [rad]

ω = Angular frequency of the input motion [rad/s]

t = Time [s]

α = Angular acceleration [rad/ s^2]

I_{xx} = Mass moment of inertia about COG [$\mathrm{kg.m^2}$]

m = Total mass of the system [kg]

l =Lever = Distance between COR & the bottom surface of tank in contact with water [m]

z =VCG= Distance between the bottom surface of tank in contact with water and COG of tank [m]

g = Acceleration due to gravity $[m/s^2]$

The resultant moment obtained from post-processing in kN.m./deg and phase obtained in degrees is converted into added mass coefficient A_{44tank} and damping coefficient B_{44tank} as follows:

$$A_{44tank} = M_R . \varphi_a . cos\ (\varepsilon) \tag{16}$$

$$B_{44tank} = M_R . \varphi_a . sin\ (\varepsilon) \tag{17}$$

Where M_R is the resultant moment in kN.m/ deg, φ_a is the roll amplitude in degrees, and ε is the phase difference in radians.

4 DESIGN AND CONFIGURATION OF TANK

4.1 Preliminary Evaluation

For the initial design of Box-shaped/ C-shaped roll damping tanks, the in-house Hoppe tool was utilized. In this tool, a tank is designed i.e. dimensions, distance from vertical center of gravity (VCG) and water level is set in such a way that the free surface moment of tank provides sufficient roll reduction to the vessel. The same in-house tool, used by Hoppe for ship tank design, was used for platform tank design, after accommodating necessary changes.

The tanks are tuned i.e. water level and tank beam is adjusted in such a way that tank period matches the eigen frequency of platform. The eigen frequencies of the platform given by FPP are presented in Table 4-1 as follows:

Table 4-1: SEAWORTHY Platform eigen periods and frequency

Motion	Eigen period [s]	Eigen frequency [rad/s]
Roll	Confidential	
Pitch		

In CFD analysis, full scale tank geometry was used. However, to validate benchmark cases, the scaled model of tank was meshed and analyzed.

Nozzle plates add internal damping in the tank and flatten the moment-phase curve, as discussed in section 1.3.1. The internal damping provided by nozzle plates depends on nozzle opening and number of plates used. Ideally, design iterations for number of nozzles and nozzle openings should be done for optimum internal damping.

4.2 Tank Configuration

Tanks were designed based on the general arrangement of Floating Power Plant's platform named SEAWORTHY, shown in Figure 4-1.

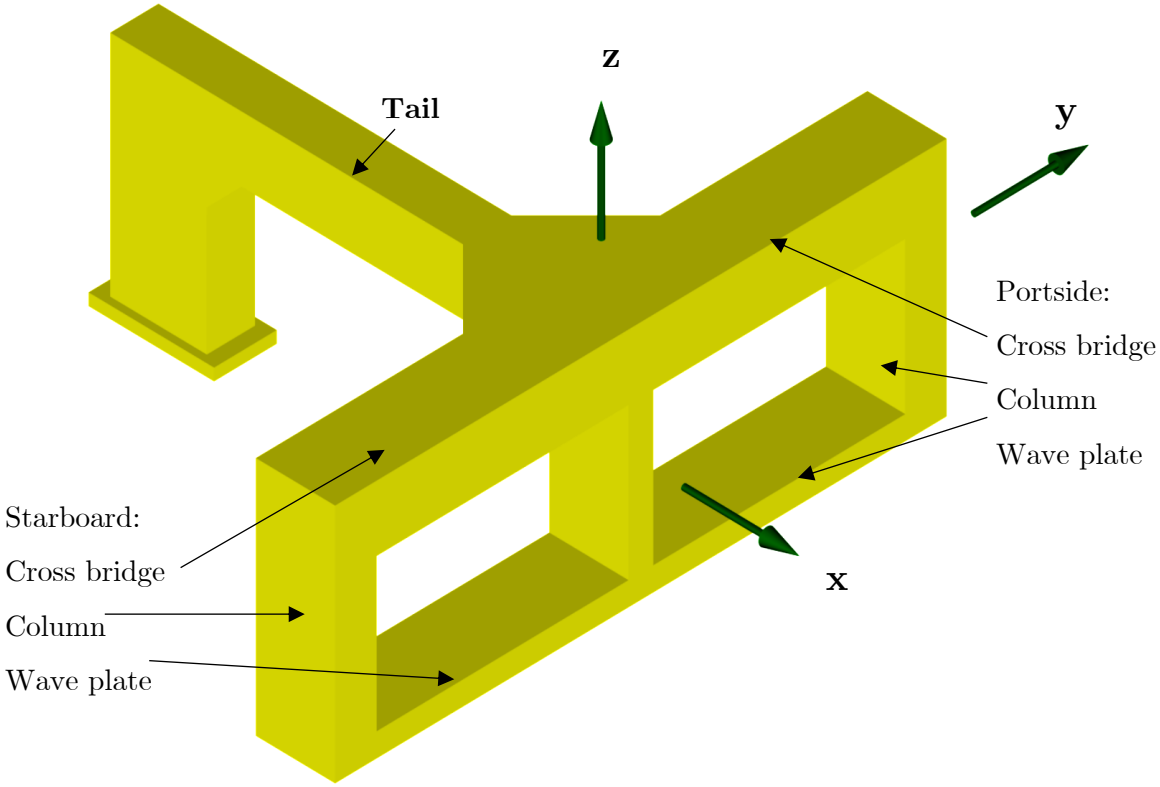

Figure 4-1: SEAWORTHY platform from FPP

The platform contains ballast in the aft, port and starboard column. Initially, both pitch damping and roll damping tanks were designed for the platform, keeping in view that the tank should be symmetric around axis of pitch or roll. The general arrangement of machinery deck is shown in Figure 4-2.

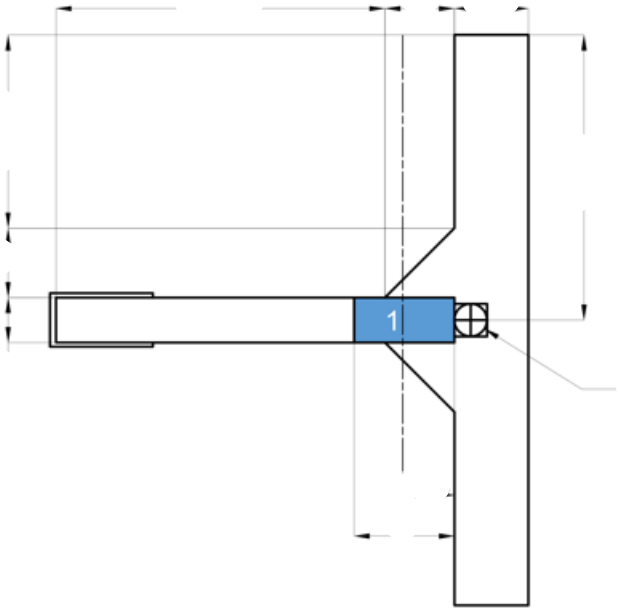

(a) Tank for pitch motion

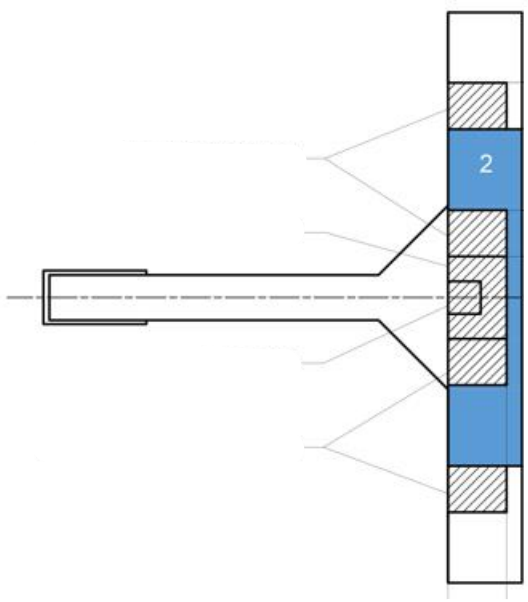

(b) Tank for roll motion

Figure 4-2: Tanks configuration in FPP platform-Top view

Both tanks extend up to the total height available in both cross bridges, as shown in the side view of Figure 4-3.

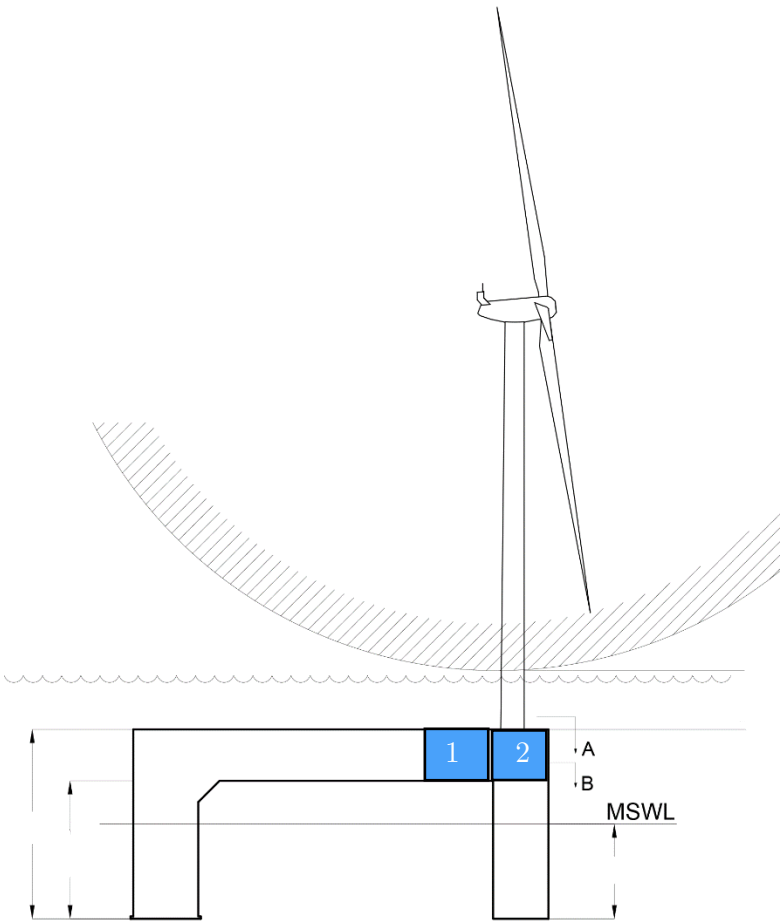

Figure 4-3: Tanks configuration in FPP platform- side view

Although both pitch and roll damping tanks can be designed for FPP platform, the pitch damping tank was not analyzed. This is because the space available for accommodating a symmetric tank around pitch axis is not sufficient for tank width; thus, will lead to very small moments and will make the pitch damping tank redundant.

For roll damping tank, the width of tank was not extended up to the full beam available in platform. It is because the extension of tank width to full platform beam gives tank height that is not sufficient to have correct tank eigen frequency.

4.3 Load Cases

The platform Wind Turbine Generator (WTG) has different load cases depending on wind direction. The wind and wave directions are considered collinear, and the turbine rotates in each wind-direction so that it faces the wind and harvests maximum energy available. The orientation for different load cases is shown in Figure 4-4 and the load cases in Table 4-2. The wind speed for mentioned load cases is 11 m/s. The displacement remains same for all load cases as the change in weight is compensated by ballast.

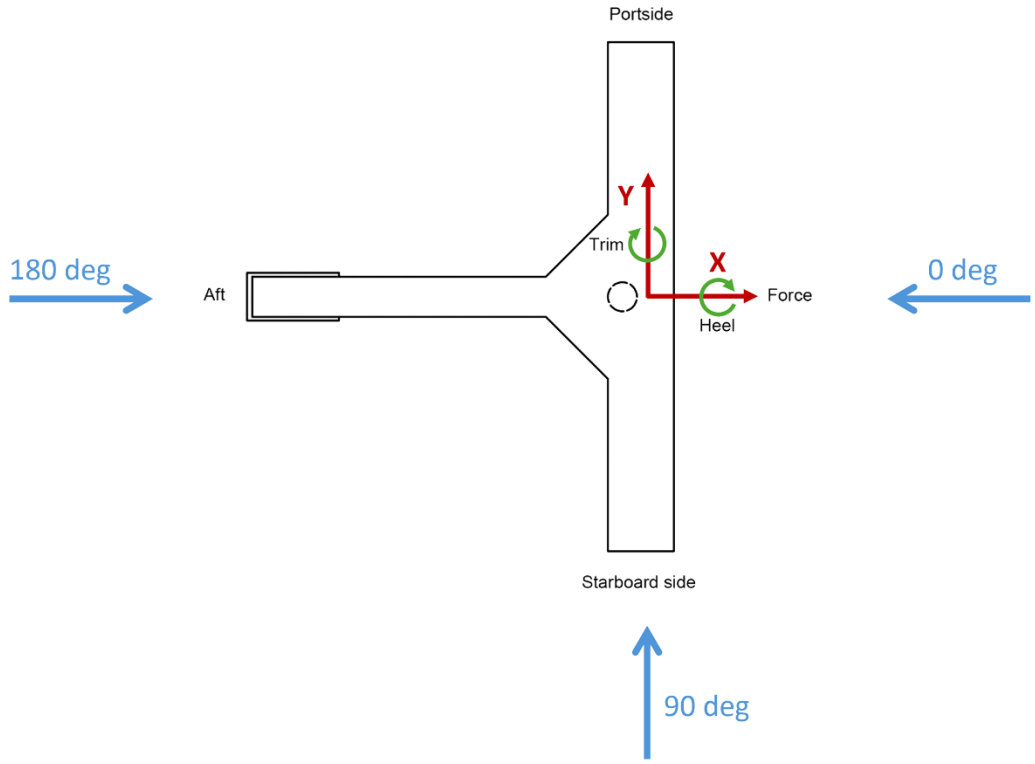

Figure 4-4: Wind turbine orientations

Table 4-2: FPP Platform load cases

Load Case	GMs [m]	Displacement [t]	Draft [m]
PROD_0			
PROD_45			
PROD_90		Confidential	
PROD_135			
PROD_180			

4.4 Selected Parameters

The design parameters of roll damping tank designed through a preliminary evaluation tool are given in Table 4-3 as shown below. It was assumed during the design that the port and starboard ballast will be replaced with mass of tank in order to keep the displacement and draft of platform constant.

Table 4-3: Tank design parameters for FPP platform

Parameters	Values
Width	44 [m]
Length	9.59 [m]
Height	7.6 [m]
Filling level	4.6 [m]
Tank period	Confidential
Tank water mass	1115.7 [t]

4.5 Design Limitations

It was found that the maximum moment that the tank can provide is limited by two factors:

1. The maximum height available for the designed tank height in the platform.
2. The total mass of port and starboard ballast available that can be replaced with tank mass, so that the draft and displacement of platform remains same.

The second factor was found to be the deciding one, and the water-level in the tank was calculated in such a way that the tank mass does not exceed the total port and starboard ballast compensation available in the platform.

5 CFD ANALYSIS

In this chapter, the methodology for developing CFD set-up to compute moment-phase diagrams of roll damping tanks is elaborated. Benchmark studies are first performed to validate CFD set-up. A parameterized model for tank designed in previous section is developed and moment-phase diagrams are computed at different water levels of the tank.

Bench model tests, currently in practice at Hoppe, have several drawbacks.

- They require fabrication of scaled models for each new design, which can take several weeks or months.
- The scaled models cannot be parametrized i.e. if design remains same, but the dimensions or aspect ratios are changed, the same model cannot be reused.
- The experimental set-up requires maintenance and use of several other software/equipment to perform the test

Roll damping moment and phase calculation via Computational Fluid Dynamics (CFD) offers several advantages over bench model tests. For simpler designs, the tank parameters can be parameterized so the same model can be reused when the dimensions are changed. CFD eliminates the need for scaling, allowing real-scale tank models to be analyzed with similar computational effort. Although the computational times can be high depending on mesh and solver used, but for a standard 3D box shaped tank geometry with internal structures and nozzles, the computation can extend upto 6 days. This is shorter than the time period required for each new model fabrication and test.

5.1 OpenFOAM

To obtain moment diagrams of the tank designed for platform, CFD analysis was performed in Open-Source Field Operation and Manipulation, OpenFOAM v2406. OpenFOAM is a C++ based computational tool, that is capable of solving continuum mechanics problems, including Eulerian multiphase model and Lagrangian particle tracking. For the present study, two solvers, interFoam and interIsoFoam were used to calculate moment at walls.

InterFoam solver is based on Volume of Fluid (VoF) method, in which each phase is represented by volume fraction. The sharp interface & surface tensions are captured by tracking volume fractions using scalar transport theorem. Solver interFoam is specifically developed for two incompressible, isothermal immiscible fluids. This solver is considered ideal for solving free-surface sloshing and wave breaking problems [35].

InterIsoFoam solver is also based on Volume of Fluid (VoF) method, however, it uses isoAdvector scheme [36]which is designed to improve accuracy of interface capturing by geometrically reconstructing the interface position and shape within the cells.

For rotating the tank around center of rotation, dynamicMesh utility is used in OpenFOAM. Dynamic mesh can be used to morph mesh at fluid interface, to create overset meshes combining two different meshes, slide mesh and move mesh along with solid body. To move

the whole domain, solid body motion solver is used in dynamicMeshDict file. There are different types of motions that can be prescribed in solid body motion. These include linearMotion, oscillatingLinearMotion, oscillatingRotatingMotion, SDA (Ship Design Analysis), oscillatingRotatingFoam and tabulated6DofMotion. Out of these motion types, tabulated6DofMotion and oscillatingRotatingMotion have been used in current study. In tabulated6DofMotion, a motion file containing time step, linear displacement vector and rotation vector are prescribed as a **`.dat`** file, which is referenced inside the dynamicMeshDict file, along with coordinates of center of gravity about which the domain will rotate. This motion type allows us to analyze different frequencies of different motions together in one simulation. In oscillatingRotatingMotion, a sinusoidal oscillating motion is prescribed with the help of center of gravity, amplitude and frequency of sinusoidally rotating object. This motion can be used for only one frequency at a time and is used to analyze motion of pendulum-like periodically rotating objects. The structure of both these input files can be found in Annexure-B.

One important parameter to be monitored for CFD analysis is Courant number or commonly called CFL number. It indicates how much information travels across a cell in unit time[37]. The courant number is calculated as:

$$CFL = \Delta t \sum_{i=1}^{n} \frac{u_{xi}}{x_i} \tag{18}$$

Where u_{xi} is velocity vector in x direction, x_i is characteristic size of mesh and Δt is time step. This shows that CFL number is highly dependent on time step and mesh size. CFL number greater than one means the information from one cell is not propagated to adjacent cell in one time step, instead it skips the cells in between and propagates to the next cell. This can lead to solutions not converging or inaccurate results that are unrealistic. With dynamicMesh, it is extremely important to control the Courant number and keep it below one, as mesh morphing without CFL control will lead to unstable solutions [38].

To validate the CFD results with experimental data, two benchmark studies were performed, before proceeding with the CFD analysis of tanks designed for platform.

5.2 Field & Martin Benchmark Study

Several Bench Model Tests (BMTs) have been performed on U-tanks for moment-phase diagram calculation, including the test by Field & Martin in 1975 (Field & Martin, 1976) and later by MARIN in 2014[40]. The tank used by Field & Martin did not have any structural restrictions while MARIN performed tests on U-tanks with and without internal damping imposed by structural restrictions. MARIN asserted that Field & Martin results underestimate moment calculation and they supported their claims by performing CFD analysis for U-tank with and without internal damping devices. MARIN used a scale of 1: 12.8 for bench model tests while Field & Martin used scale of 1:14.5.

In 2016, Hoppe performed bench model tests along with CFD analysis for U-tank without restrictions, with the same scale i.e. 1:14.5 (with some tolerances) and geometry as that of Field & Martin. In present study, the results of 2D and 3D analysis in OpenFOAM are compared with bench model tests of U-tank without lid, used by Field & Martin, MARIN and Hoppe US

& German facility. The real and model-scale tank dimensions, along with symbols used can be found in Table 9-3 in Annexure-B. The U-tank used in bench model tests in Hoppe, identical to the one used by Field & Martin, is shown in Figure 5-1.

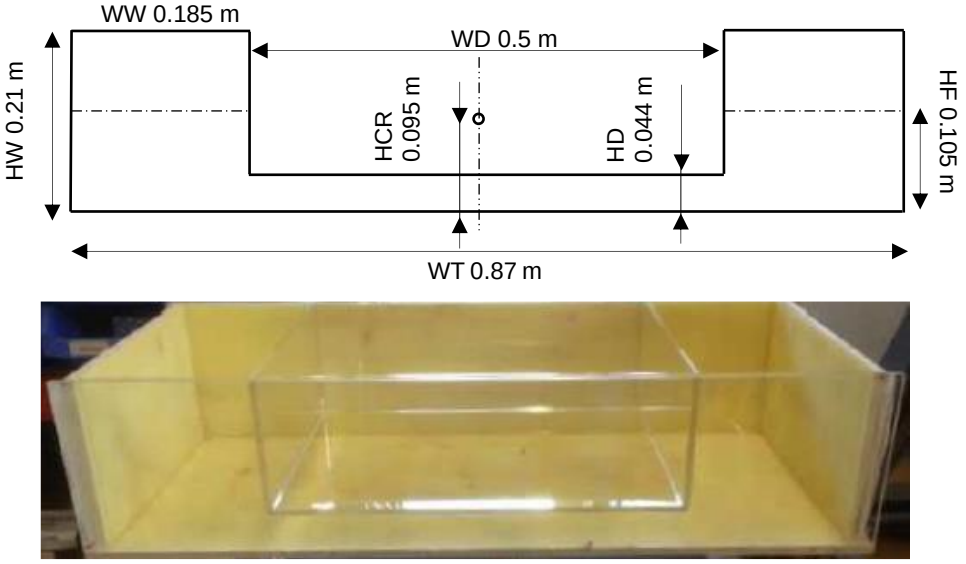

Figure 5-1: Field & Martin U-tank with no lid (model scale 1:14.5)

5.2.1 Convergence Study

Convergence study for three different mesh sizes at resonance frequency was performed. Although the convergence study for time step is beneficial to reduce computational time of one case, it was skipped to reduce overall computational time taken and a time step of 0.01 s was selected. The courant number limit was set to 0.5 in solver settings to avoid CFL exploding due to inaccurate selection of time step. It was observed that 0.01 s gave sufficient convergence of solution with courant numbers well below one. The mesh sizes were taken from simulation matrix of benchmark test cases already performed for Field & Martin tank (Hoppe database).

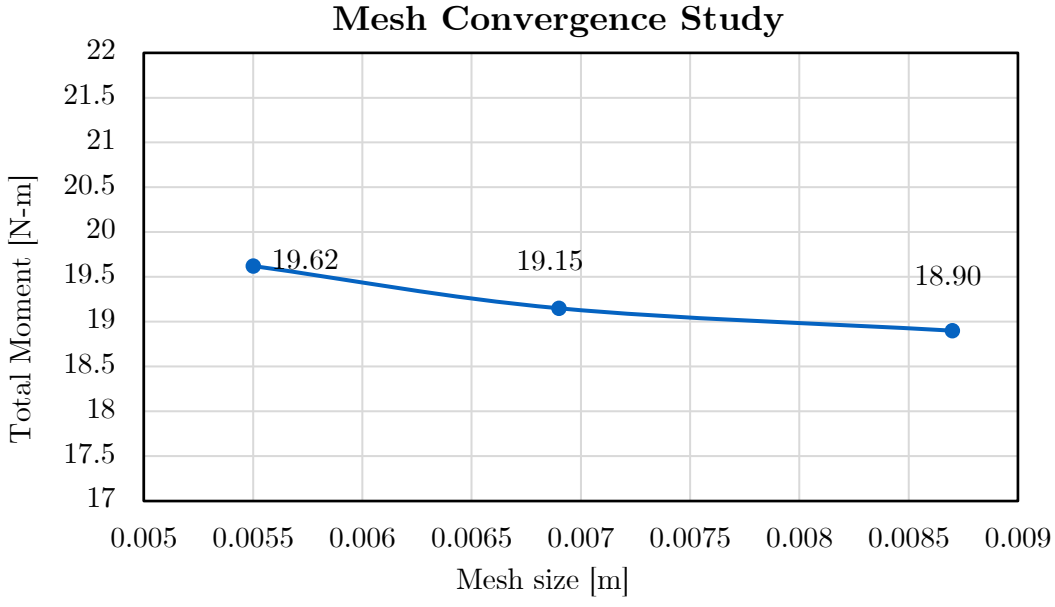

Figure 5-2: Convergence study for Field & Martin tank at 2.67 rad/s resonance frequency

The convergence study for total tank moment was performed for 0.0055 m mesh size corresponding to 159 cells in width, 0.0069 m mesh size corresponding to 126 cells in width and 0.0087 m mesh size corresponding to 100 cells in width of tank. Fourier transformation of total moment in time domain was performed, at resonance frequency and the peak amplitude of total tank moment for each mesh was plotted, as shown in Figure 5-2. From the plot, the moment given by refined 0.0055 m mesh is a bit larger and closer to peak resultant moment value of 20 N-m obtained in original Field & Martin test, as discussed in sub-sequent section 5.2.4. Therefore, this mesh was used in further analysis for validation.

5.2.2 Pre-Processing

In OpenFOAM, interFoam multiphase solver was used to calculate moments through time domain analysis. The sloshing tank tutorial present in openFOAM was modified to calculate forces and moments at walls as a function object. Parametrized blockMesh was made for the given U-tank. Dynamic mesh with tabulated6Dof was used to input the motion file of tank at different frequencies. The motion file is same as the one used for bench model tests. It contains a regular sinusoidal motion which includes gradual change of frequencies through ramp function. The transition period, where the frequency is changed from one to another in motion file, is later clipped out in post processing. The frequency range used varies from 1.53 rad/sec to 3.82 rad/sec. Reynolds-Averaged Navier-Stokes (RANS) model was used for turbulence and wall functions were defined at each boundary. The simulation parameters of Field & Martin benchmark model at model scale are shown in Table 5-1.

Table 5-1: Simulation parameters of Field & Martin benchmark study at model scale

Simulation Parameters	Values
Model scale	1:14.5
Time step	0.01 s
Write Time	0.01 s
Max Courant No. /CFL number	0.5
Roll amplitude	2°
Frequency range	1.53 – 3.82 rad/s
Solver	interFoam, interIsoFoam
Turbulence model	k-epsilon
Mesh size	0.0055 m
Mesh aspect ratio	1
Cells	3,104
Water level	0.105 m
Lever (from tank bottom to CoG)	0.095 m

Gauss van Leer scheme was used for volume fraction which is a second order method that reduces numerical diffusion and provides better accuracy than upwind or central differencing schemes [41]. The meshed domain along with water level is shown in Figure 5-3 below.

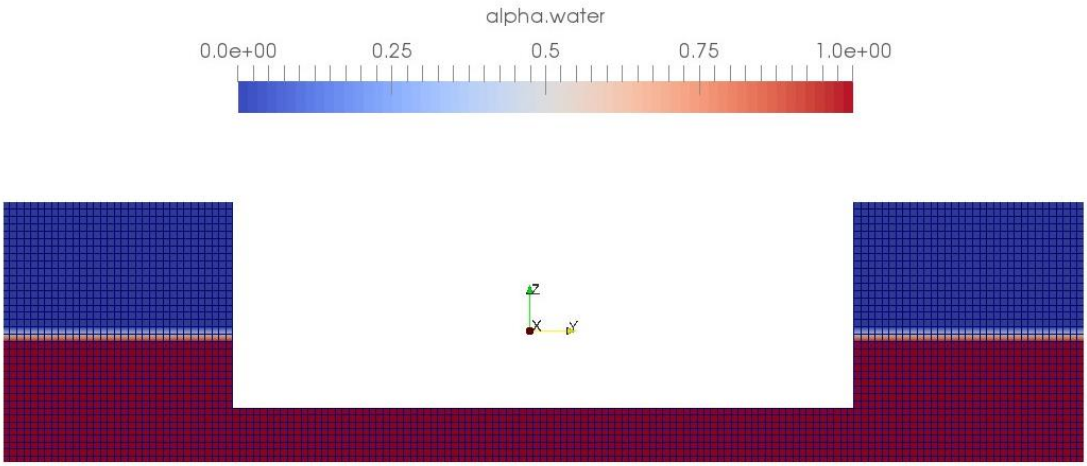

Figure 5-3: Meshed domain of Field & Martin Benchmark study

5.2.3 Post-Processing for Resultant Moment

The moment calculated through bench model tests are the resultant moments obtained after subtraction of tare moment. A MATLAB script is generated that calculates the tare moment for each frequency, as shown in section 3.2, and calculates the resultant moment by conversion time domain results into frequency domain via FFT. Simulations were carried out using interFoam and interIsoFoam for both 2D and 3D models, as shown in Figure 5-4.

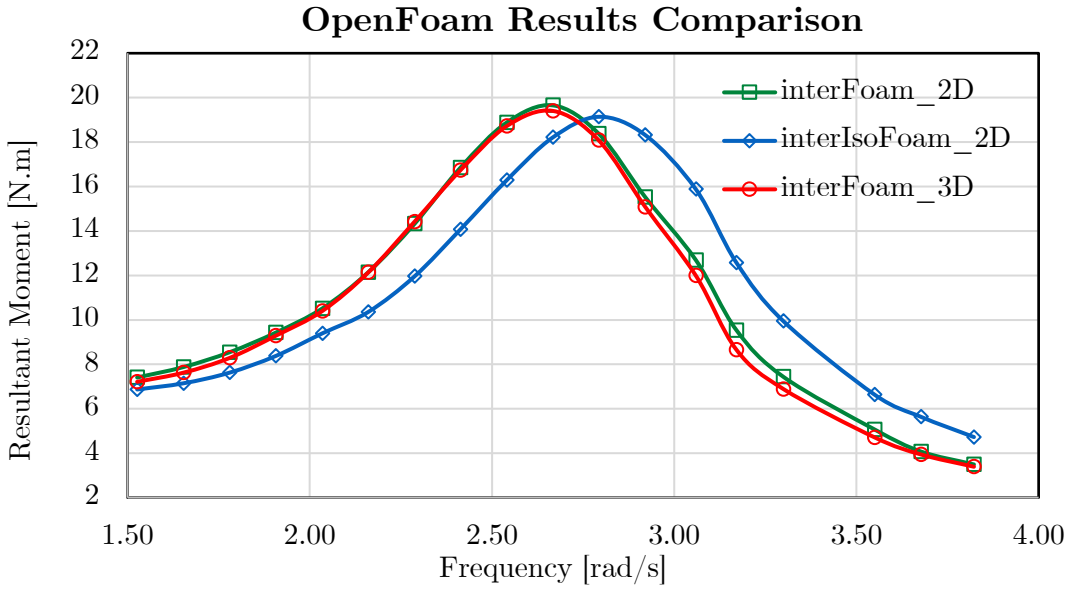

Figure 5-4: Moment diagram of Field & Martin tank OpenFOAM analysis (model scale)

It can be seen from the graph that the resultant moment calculated from 3D and 2D domains are almost identical. It is because the tank is symmetric along its length and there are no internal structures changing the flow. As 2D analysis assumes that flow properties are uniform in third dimension, this assumption fits well for the current tank under study, with no internal

structures. The plot also shows that with interIsoFoam, there is a phase shift, although same numerical schemes and parameters were used as interFoam. One reason for this phase difference produced can be explained by high mesh sensitivity of interIsoFoam. InterIsoFoam is designed to capture detailed interface dynamics and if the mesh is not fine at interface, it can lead to inaccurate results. This implies that it requires mesh morphing at air-water interface in the tank, in addition to tank rotation. This can exceptionally increase the computational time and power required. Furthermore, interIsoFoam requires more careful tuning of numerical schemes and is not as robust as interFoam, which is used for wide range of multiphase flow problem and can handle numerical instabilities.

5.2.4 Comparison of Results

The results from OpenFOAM were compared with experimental bench model tests performed by Hoppe-US facility, Hoppe-German facility, MARIN and with the Field and Martin benchmark. The comparison plot is shown in Figure 5-5.

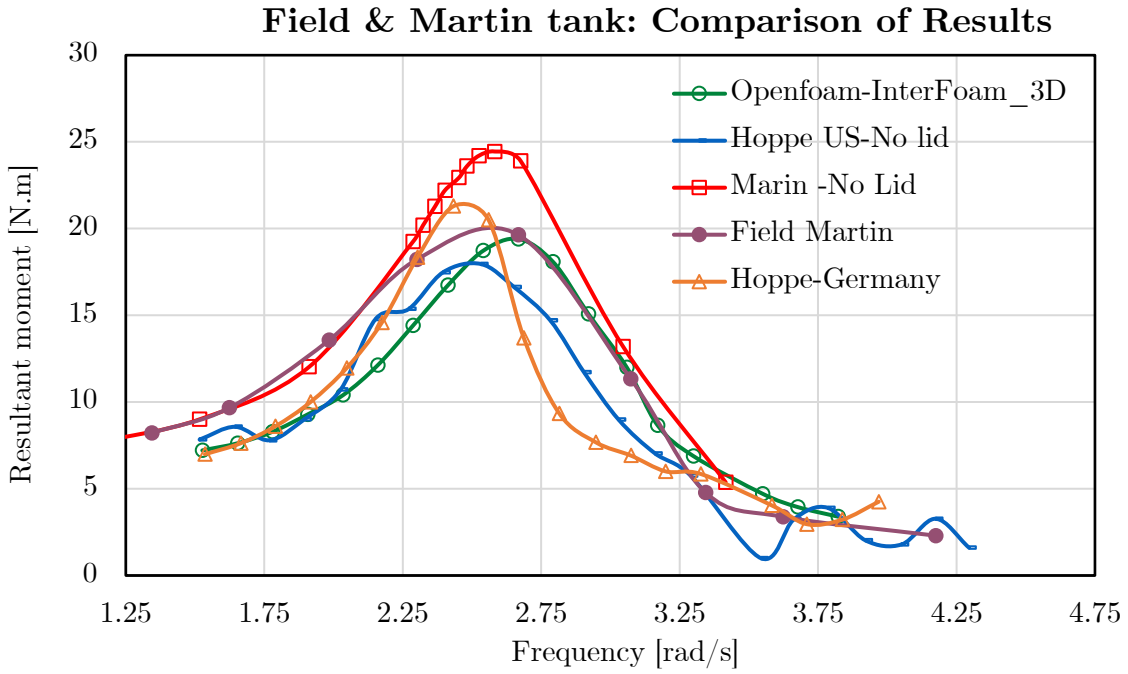

Figure 5-5: Comparison of Field & Martin OpenFOAM results with previous tests at model scale

It can be seen that OpenFoam results lie in close proximity with original Field & Martin results. However, compared to Hoppe results, it has a peak shift. With the use of interIsoFoam, the peak shift further increases, as shown in Figure 5-4; hence interFoam results are considered more reliable. It can be seen that previous bench model tests of Field & Martin have variations as well, although the peak moment values for all tests match, except for MARIN which has a very high peak. Due to the lack of a consistent pattern in previous benchmark model results, drawing definitive conclusions from this benchmark analysis about the conformity between OpenFOAM results and experimental moment diagrams is challenging. Hence, another benchmark study was performed to validate the OpenFOAM solvers and case files for moment diagram calculation.

5.3 Hermes Tank Benchmark Study (3D Analysis)

To further validate CFD results from OpenFOAM, another benchmark study was performed on a tank from a project HERMes, shown in Figure 5-6. The details of tank dimensions for real and model scale can be found in Table 9-4 in Annexure-B.

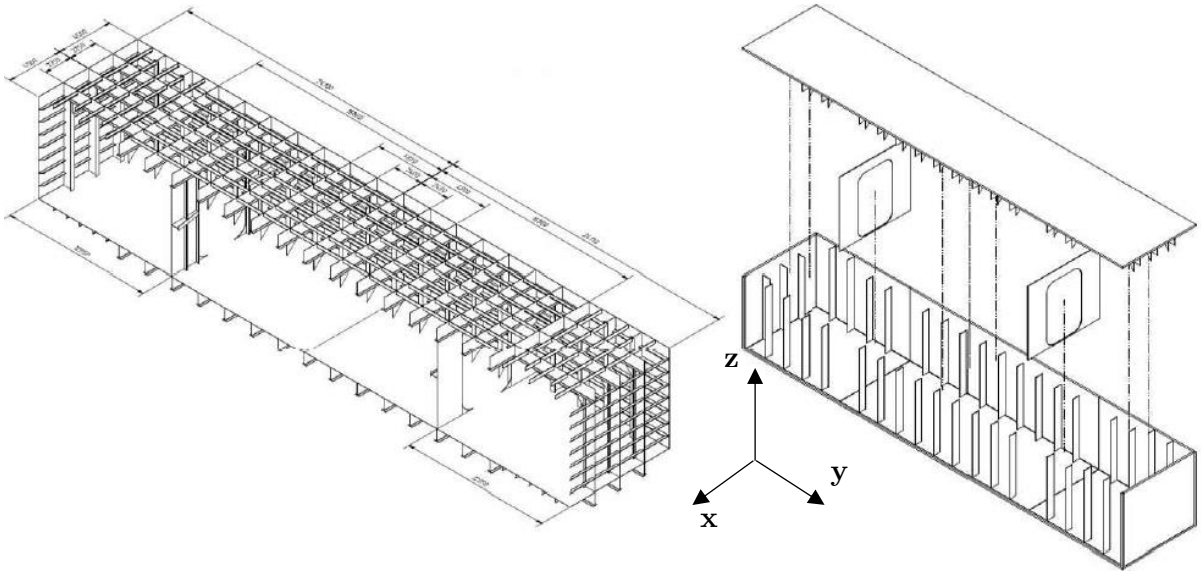

Figure 5-6: HERMes benchmark tank

5.3.1 Pre-Processing

Before running the case files, the geometry of Hermes tank needs to be meshed. As evident, to develop a structured mesh for such complex geometry is not possible, hence OpenFOAM's internal meshing tool called snappyHexMesh was used. For snappyHexMesh, a background structured mesh is developed, and an imported surface file of the geometry is defined. The feature edges are extracted from geometry file and the geometry is snapped out of background mesh. Symmetrical properties of the tank geometry were applied, to save computational time. Same numerical schemes as Field & Martin tank's analysis were used in fvSchemes of HERMes tank analysis. The meshed geometry and the meshing of water-air interface is shown in Figure 5-7. The simulation parameters used are shown in Table 5-2.

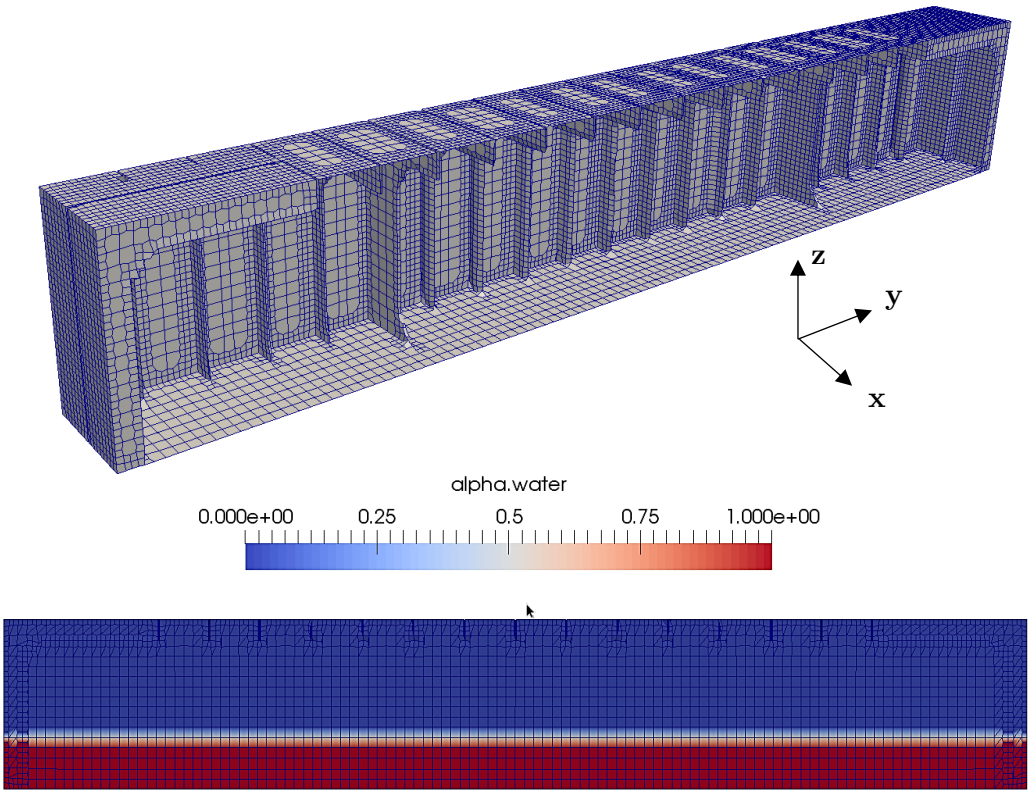

Figure 5-7: HERMes tank meshed domain in OpenFOAM

Table 5-2: HERMes tank simulation parameters at model scale

Simulation Parameters	Values
Model scale	1:26
Time step	0.01 s
Write Time	0.01 s
Max Courant No. /CFL number	0.5
Roll amplitude	2°, 5°, 10°
Frequency range	0.353 – 3.2 rad/s
Frequency No.	19
Solver	interFoam, interIsoFoam
Turbulence model	k-epsilon, k-omega SST
Background Mesh size	0.0154 m, 0.0103 m
Cells	30,254 for 0.0154 m mesh size 78,714 for 0.0103 m mesh size
Water level	0.0969 m
Lever (from tank bottom to CoG)	-0.374 m

5.3.2 Revised OpenFoam Workflow

For Hermes tank analysis in OpenFOAM, solid motion type tabulated6DofMotion, using motion file was not used, since the transition period from one frequency to another caused divergence in solution for Hermes tank. Instead, a different methodology was used where case files were developed for each combination of roll amplitude and frequency. The solid motion type OscillatingRotatingMotion was used where each frequency is defined in separate case folders. A bash script was developed to first copy the main case folder and produce copied folders such that each folder represents one combination of simulation matrix, shown in Table 5-3.

Table 5-3: Simulation matrix for CFD analysis

	Roll Amplitudes			
Frequencies		2°	5°	10°
	Freq 1	2° , Freq 1	5° , Freq 1	10° , Freq 1
	Freq 2	2° , Freq 2	5° , Freq 2	10° , Freq 2
	Freq 3	2° , Freq 3	5° , Freq 3	10° , Freq 3

A total of 19 frequencies were used with three different roll amplitudes of 2°,5° and 10°, which leads to simulation matrix size of 57 simulations. Another parameter of water level can also be added in this simulation matrix; however, it was skipped to save computational time in current study. A frequency range of 0.353-3.2 rad/s was used. The end time of simulation for each case folder was set to be equal to time required for 10 oscillations at each frequency. The bash script shown in Annexure-B not only copies parent case files according to total number of elements in simulation matrix, it also goes inside dynamicMeshDict folder defining the mesh motion in each copied folder, changes the roll amplitude and frequency value according to each element of simulation matrix and then executes the batch script for running all copied case folders in queue, utilizing maximum CPU power available.

For this time-consuming computation, a 28-core computational node was employed and SLURM was used to run all case files in queue, with each simulation utilizing 4 cores. It was found that 0.0154 m background mesh with K-epsilon turbulence model took around 23 hours in computation through this workflow.

5.3.3 Post-Processing for Resultant Moment

The simulations performed for each frequency case folder for 10 oscillations was then processed in MATLAB. Mass properties required for tare moment calculation were taken from Hoppe database. Fourier transform analysis was performed to convert each frequency's time domain results into frequency domain and the resultant moment for full tank was calculated after subtracting tare moment. Since the model is scaled, the real scale moment is calculated as:

$$\omega_{Real} = \frac{\omega_{model}}{\sqrt{\lambda}} \tag{19}$$

$$M_{Real} = \lambda^4 . M_{Model} \tag{20}$$

Where λ is scale factor of model. The phase at each frequency is calculated by Fourier transformation. The OpenFOAM results after conversion to real scale and its comparison with bench model test (BMT) are shown in Figure 5-8.

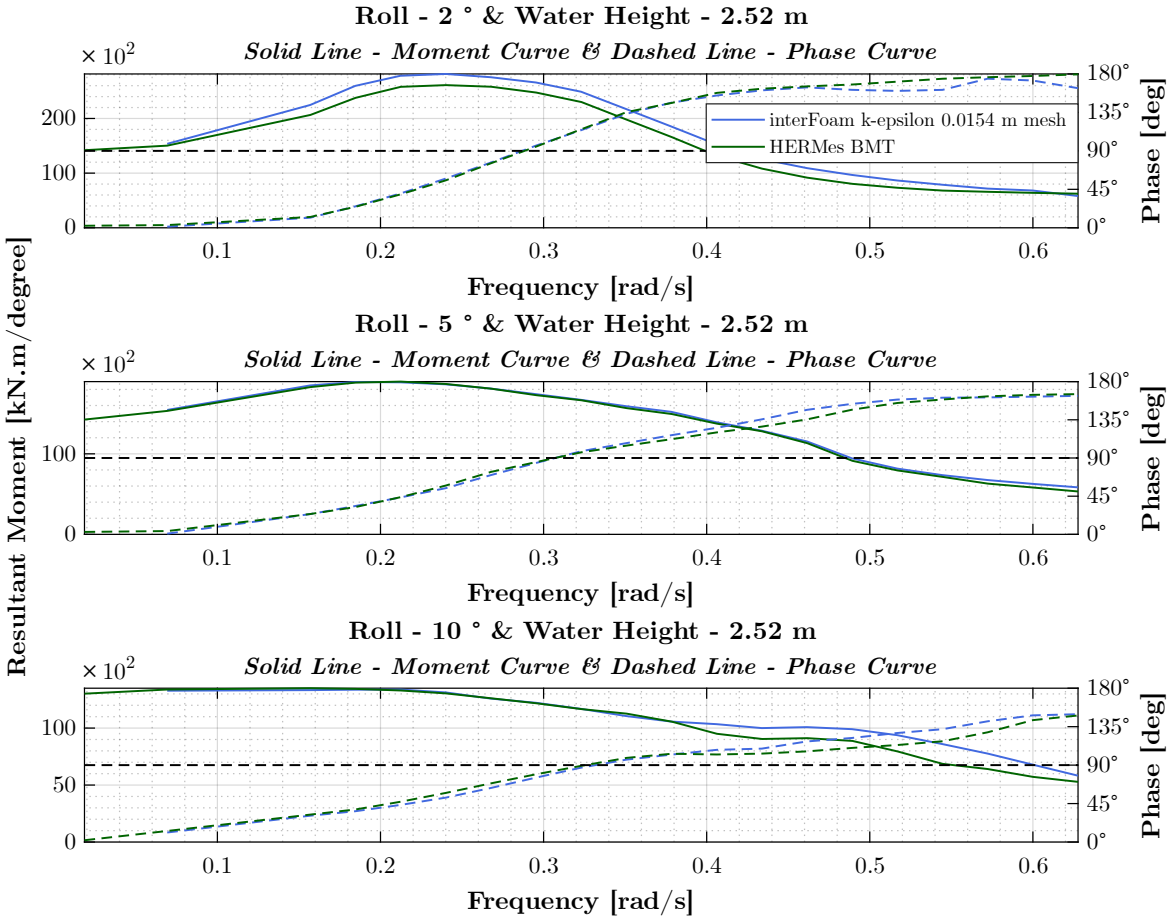

Figure 5-8: Comparison of HERMes OpenFOAM results (real scale) with BMT (real scale) at 0.0154 m mesh with k-epsilon modeling

As seen from the plot, the OpenFOAM results are reasonably close to Bench Model Test (BMT) results from the experimental bench in Hoppe at 5° and 10° roll amplitudes. However, there are some discrepancies between BMT and OpenFOAM results at higher frequencies. For 2° roll amplitude, there is an offset between BMT and OpenFOAM resultant moment at all frequencies. For interFoam results with k-epsilon model and 0.0154 m mesh, there is percentage difference of 7.82% at resonance, which increases to 20% at 0.49 rad/s frequency. To reduce this difference in resultant moment, another study with different turbulence model of k-Omega SST was tried in OpenFOAM. To see the possibility of mesh causing the offset, a refined mesh of 0.0103 m was also investigated.

5.3.4 Comparison of Results

After further investigation with different turbulence models and mesh sizes, the plots at real scale are compared as shown in Figure 5-9. It can be seen that for 2° roll amplitude, k-epsilon model with refined mesh of 0.0103 m gives the least offset in resultant moment. It also gives reasonable conformity with BMT results for phase diagram and performs better at higher frequencies for 5° and 10° roll amplitudes. Turbulence model k-omega SST gives the least accurate results for resultant moment. At 10° roll amplitude, k-omega SST model performs better for some higher frequencies but then the offset in resultant moment becomes larger as the frequency increases. The percentage difference between BMT results and OpenFOAM interFoam results of 0.0154 m background mesh with k-epsilon, k-omega SST and 0.0103 m background mesh with k-epsilon turbulence model is shown in Annexure-B. It can be inferred with current benchmark study that interFoam solver with k-epsilon turbulence model performs best and the results improve with increased mesh refinement. In terms of the phase diagram, all models exhibit minor deviations from the BMT phase diagram. However, the overall phase results from the CFD analysis align closely with the BMT results.

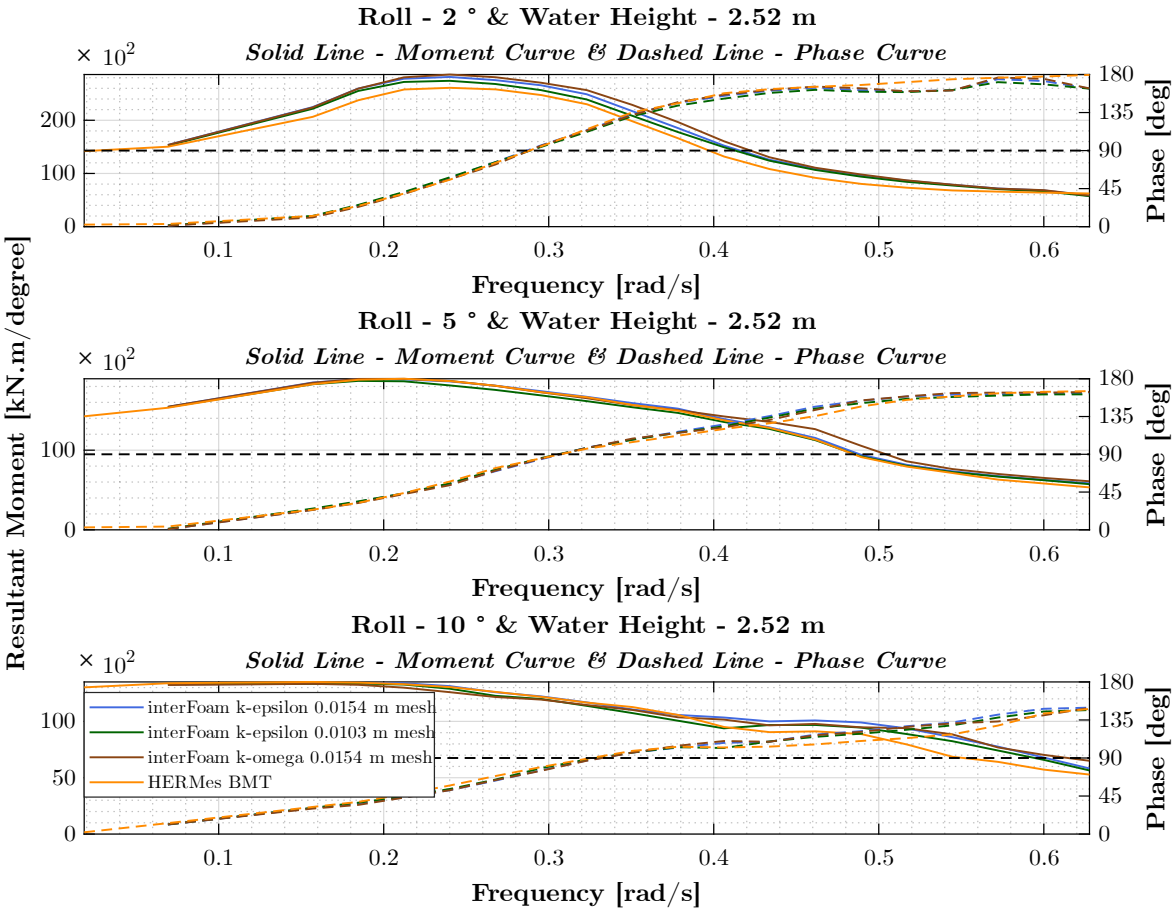

Figure 5-9: Comparison of Hermes OpenFOAM results (real scale) with BMT (real scale) at different mesh & turbulence models

5.4 FPP Platform Tank Analysis

For the roll damping tank designed for FPP's platform SEAWORTHY, a parametric mesh is to be developed in OpenFOAM, so that different tank dimensions can be tested to find the optimum design. Since the mesh produced by snappyHexMesh relies on external geometry surface file, it cannot be used for parametrization of tank geometry. A mesh generator tool called Gmsh [42], which is compatible with OpenFOAM, was used to generate a parameterized tank model. Two nozzles were used in the C-shaped parametric tank design and the parameters of tank length, breadth, height, C-shaped cut-out, grid size, nozzle opening and nozzle location from centerline were parameterized. The tank geometry developed via Gmsh tool and its meshed domain is shown in Figure 5-10.

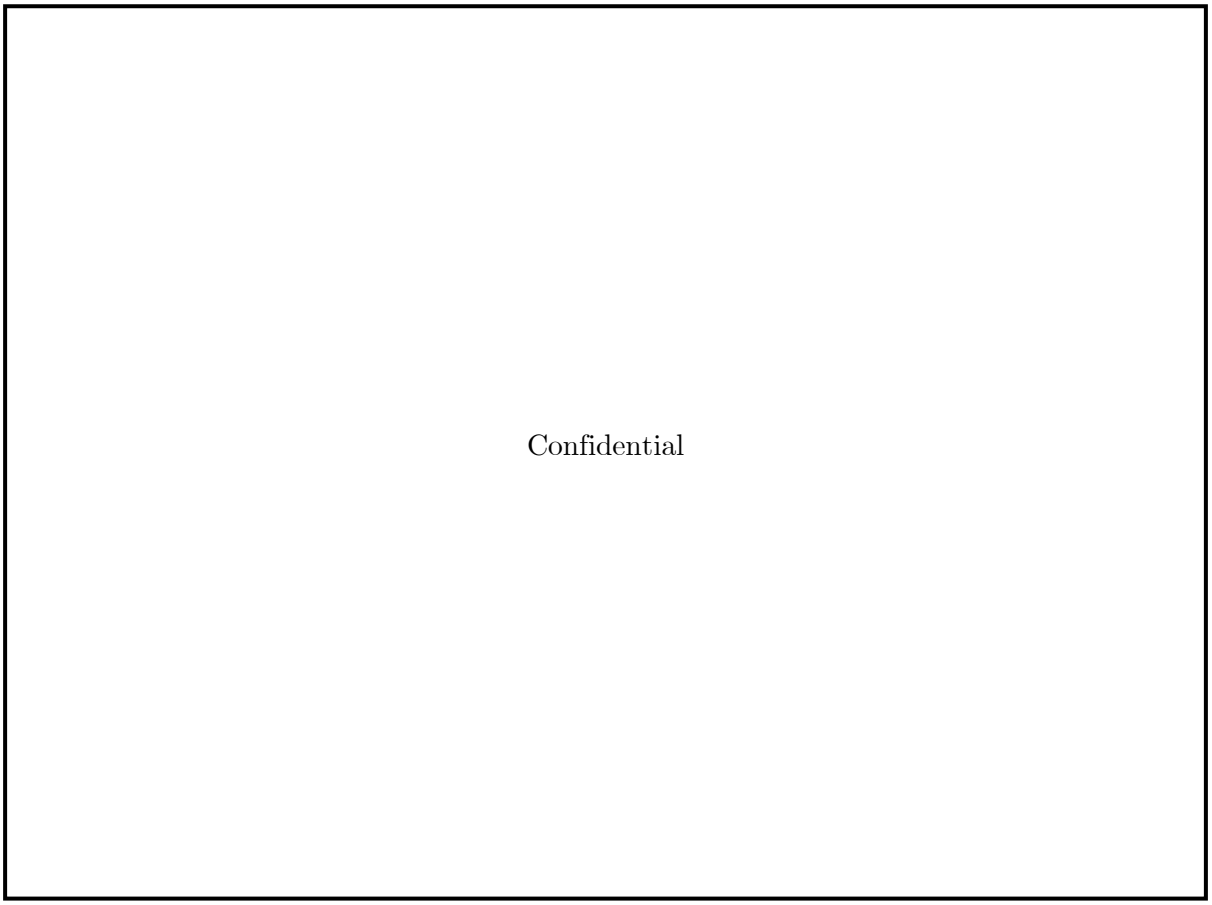

Figure 5-10: Meshed domain of designed tank for FPP platform

The simulation parameters used in platform tank CFD analysis are mentioned in Table 5-4. The processing in OpenFOAM for platform tank analysis was performed with the same methodology as HERMes tank, discussed in section 5.3.2 and 5.3.3. The same processing and post-processing scripts, developed for HERMes benchmark study were used for platform tank analysis to ensure that no errors arise due to incorrect methodology or scripts. As benchmark studies presented in previous sections have demonstrated that the interFoam solver with k-epsilon turbulence modeling produces more realistic results, the same were used in current platform tank analysis as well.

Table 5-4: Simulation parameters for FPP platform tank analysis at full scale

Simulation Parameters	Values
Scale	1:1
Time step	0.01 s
Write Time	0.01 s
Max Courant No. /CFL number	0.5
Roll amplitude	2°, 5°, 10°
Frequency range	[redacted] rad/s
Frequency No.	21
Solver	interFoam
Turbulence model	k-epsilon
Mesh size	0.5 m
Cells	14,400
Water level	4.6 m, 2.8 m
Lever (from tank bottom to CoG)	2.73 m for 4.6 m water level 0.66 m for 2.8 water level

5.4.1 Post-Processing for Resultant Moment

The time domain results of designed tank at each frequency are converted into frequency domain via FFT in MATLAB. For post-processing, mass properties calculated for designed water levels (shown in Table 9-6 in Annexure-B) are used for tare moment calculation. The resultant moment-phase diagram of designed tank, after subtraction of tare moment, is shown in Figure 5-11. The resultant moment values for different roll amplitudes at 90° phase difference is tabulated in Table 5-5.

Table 5-5: Resultant moment values at designed tank's eigen frequencies

Roll Amplitude [°]	Tank frequency at 90° phase difference [rad/s]	Resultant moment [N.m]
2	Confidential	3.710E+07
5		4.880E+07
10		5.476E+07

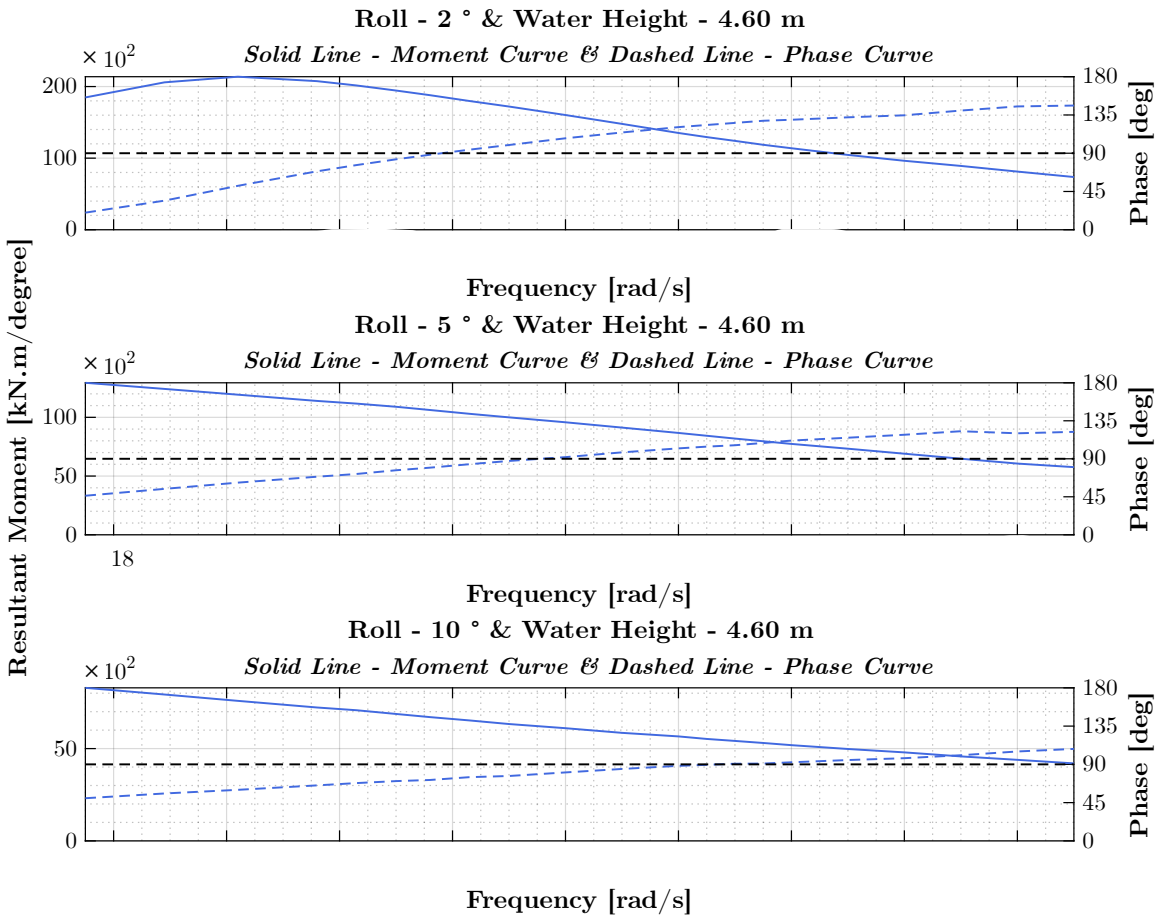

Figure 5-11: Moment-phase diagram of designed tank (CFD results at real scale)

As discussed in section 4.1, the tank needs to be designed in the in-house tool for preliminary design evaluation in such a way that it's eigen period matches with eigen period of platform at 5° roll amplitude. However, during sea-keeping analysis of platform with RDT (discussed in section 6.7), it was observed that the roll eigen frequency of platform changes with integration of tank. The new roll eigen frequency of platform with tank was calculated to be around [redacted] rad/s. In the in-house tool, the water-level that leads to tank period identical to platform's new eigen frequency of [redacted] rad/s was found to be 2.8 m. Hence another CFD analysis for 2.8 m water-level was performed and the results of both water-levels were compared, as shown in Figure 5-12.

From the plot, it can be seen that the new water level of 2.8 m gives lower resultant moment in the desired frequency range while 4.6 m water level gives higher moment at all desired frequencies. A higher water-level of 4.6 m was hence used to obtain maximum resultant moment around 90° phase difference. A water-level higher than 4.6 m leads to tank mass exceeding the ballast compensation available. Hence the water-level cannot be further increased for the designed tank.

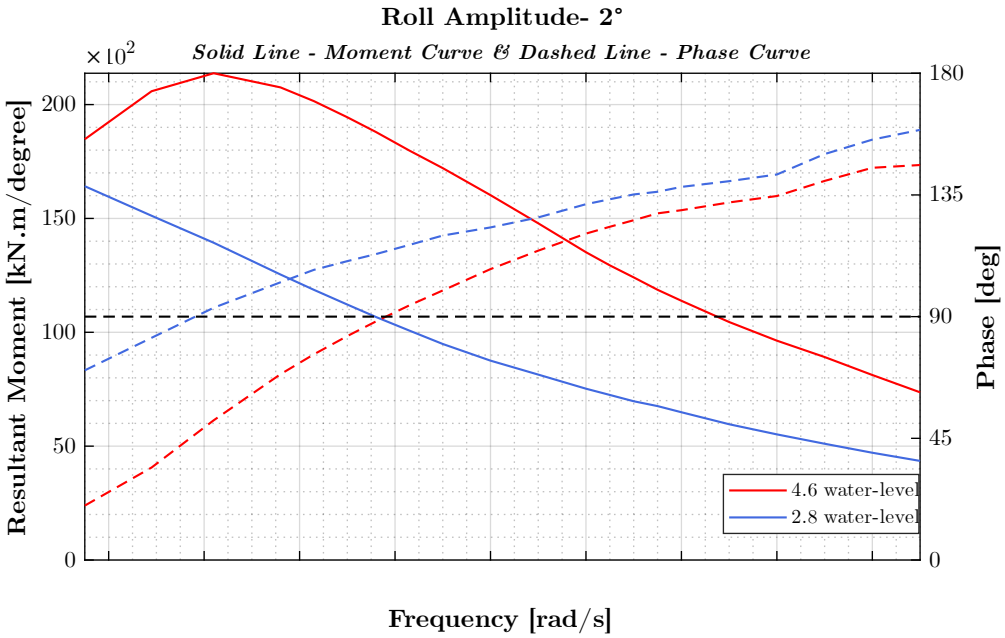

Figure 5-12: Effect of water level on moment-phase diagram of RDT designed for FPP

When water level of tank is changed, the VCG of platform changes due to different mass distribution. Consequently, the lever i.e. distance from center of gravity of platform to tank bottom also changes. Variation in VCG leads to variation in transverse GM and hence the roll stiffness of platform also changes. This indicates that changing the water-level in tank leads to iteration of both the CFD set-up and sea-keeping analysis.

6 SEA-KEEPING ANALYSIS

In this chapter, sea-keeping analysis of the platform is conducted using potential theory. The roll RAO of platform, in the absence of RDT, is obtained from this analysis and compared with the data provided by FPP. The effect of tank mass and change in roll stiffness of platform due to tank addition is investigated. A new roll RAO is computed, accounting for these factors. The resultant moment obtained from CFD analysis of designed tank is applied as added mass and damping coefficients to the updated roll RAO obtained. Finally, the percentage reduction in roll is calculated to evaluate the effectiveness of the tank design. In this report, the roll RAO of the platform, which includes the tank mass and the altered roll stiffness but excludes the added mass and damping coefficient from the tank moment, is referred to as the un-stabilized RAO of the platform with the tank.

6.1 Boundary Element Method

In boundary element method, the fluid velocity potential is calculated by solving boundary integral equation on the surface of body only, instead of whole domain volume. This significantly reduces the computational time and transforms three-dimensional potential flow problem around a body into two-dimensional problem of source distribution. Boundary element method, also known as panel method, has two variants for linear sea-keeping.

1) Green function panel method: In this method, the free surface boundary condition is already satisfied by constant and pulsating source distributions, therefore the free surface does not need to be covered by panels and only the boundary condition on body needs to be satisfied.
2) Rankine panel method: In this method, the body boundary condition, free-surface condition and the radiation condition have to be satisfied numerically. Hence the free surface around the body needs to be covered by panels as well. [43]

NEMOH (developed by Ecole centrale de Nantes) is an open-source boundary element solver for potential flow analysis, designed to compute first-order hydrodynamic coefficients in the frequency domain. It also has a provision to accommodate viscous damping and added stiffness of mooring. It uses green function based on Delhommeau's formulation [44]to formulate Boundary Integral Equation (BIE). The BIE is then discretized using the constant panel method and diffraction & radiation potential along with corresponding velocities are solved at each panel. In the end, hydrodynamic coefficients of added mass and damping coefficients are integrated over the body surface using the diffraction and radiation potentials calculated in previous step. NEMOH assumes zero forward speed, and regular waves in its sea-keeping analysis. The normalized Response Amplitude Operator (RAO) generated by NEMOH exhibits a linear relationship with wave amplitude. However, in reality, this relationship is non-linear. For the purposes of the current study, the non-linear effects can be disregarded due to the flat surfaces of the platform columns.

6.2 NEMOH Case Folder Structure

The NEMOH case folder is organized to include several key components necessary for the analysis of the platform. This folder contains:

1. Mechanics Folder: This folder holds matrices for inertia, stiffness, added damping, and added stiffness, which are computed by NEMOH based on the center of gravity (CoG) specified in the mesh configuration file.
2. Motion Folder: This folder includes files related to the platform's motion e.g. RAO.
3. Configuration Files: This category includes the files for mesh generation, NEMOH configuration file and an input solver file. These contain the information about number of panels, motion settings, generalized forces about a reference point, frequency range and wave directions, post-processing functions and quadratic transfer function flags.

NEMOH recommends that the same reference point should be used for all forces and moments used in configuration file. The inertia & stiffness matrices should also be provided at the same reference point for RAO computation. Since the hydrostatic output files for inertia and stiffness matrices are calculated at the center of gravity (CoG), it implies that NEMOH necessitates the response amplitude operators (RAOs) to be determined at CoG rather than at any other point.

6.3 Pre-Processing

NEMOH requires the mesh to be input in a specific format. NEMOH documentation [45] recommends using external mesh conversion tool called meshMagick to convert surface files into formats compatible with NEMOH. It is required that only the immersed part of body should be defined in mesh file and the body part above waterline should be cut out. For this purpose, the geometry of platform was first cut in Rhinoceros 3D and then meshed via quadrilateral meshing. Three different structured meshes, symmetric about x-axis, were developed with different number of panels, as discussed in the subsequent section. The cut geometry with a quadrilateral mesh is illustrated in Figure 6-1. Since only roll damping tank is to be analyzed, the wave direction was set to be 90° i.e. only beam waves were considered.

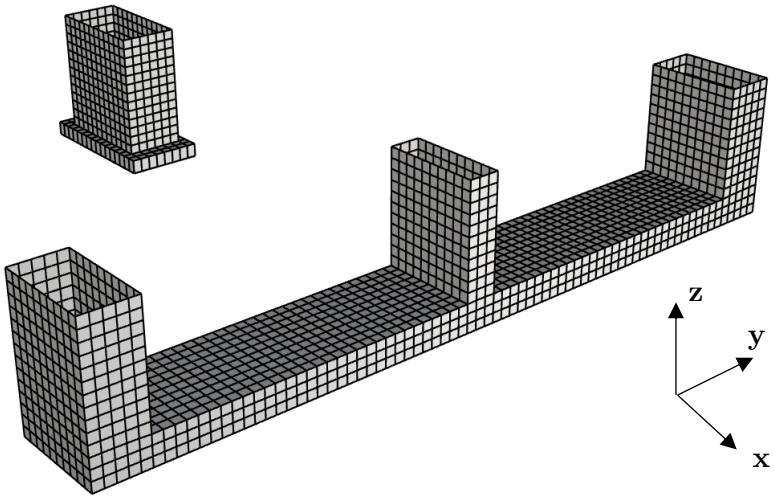

Figure 6-1: Meshed surface of platform in Rhinoceros

The analysis data and results provided by FPP for SEAWORTHY is based on origin point of platform instead of CoG. NEMOH produces mass and stiffness matrices at CoG and consequently the RAO is also recommended to be calculated at CoG. To eliminate discrepancies arising from using different reference points for hydrostatic and hydrodynamic coefficients calculations, the mass and stiffness matrices employed by FPP in their sea-keeping analysis were utilized.

6.4 Mesh Convergence Study

Mesh convergence study was performed for roll Response Amplitude Operator (RAO) of the FPP platform without viscous damping, as shown in Figure 6-2. Since the roll eigen frequency of un-stabilized platform (platform without RDT) mentioned in Table 4-1 corresponds to resonance frequency of [redacted] rad/s, the mesh convergence was performed for frequencies around this peak. From the graph, it can be seen that 1263 and 2018 panels give same plots while 3526 and 4035 panels give identical plots. This is because these pairs have similar number of panels on columns in-y direction, as shown in Figure 9-2 in Annexure-C. Since no viscous damping is used in this analysis, the resonance peak will keep on increasing based on frequency step size and number of panels. Both 1263 and 2018 panels give peaks that are closer to FPP peak while the more refined mesh with 3526 and 4035 give peak higher than FPP results. The mesh with 1263 panels was then selected for further analysis, as it leads to least computational time and gives results identical to 2018 panels.

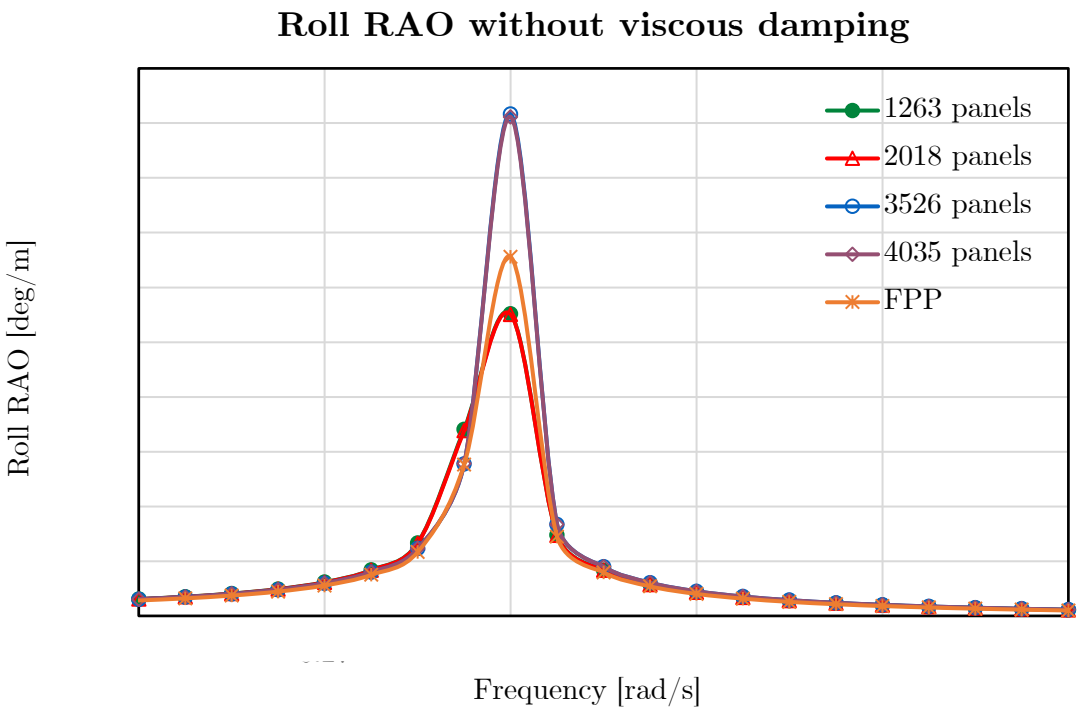

Figure 6-2: Mesh convergence study for platform without tank

6.5 Workflow in NEMOH

In NEMOH, RAO is calculated using equation 12, which is reiterated as follows:

$$\{-[M + M_{add}(\omega)]\omega^2 - i\omega[\ B(\omega) + B_{add}] + [K_h + K_M]\}\ X(\omega) = F_E(\omega) \tag{21}$$

Viscous damping and stiffness imparted by mooring are added in B_{add} and K_M matrix. Both of these matrices do not depend on frequency and their values are considered constant for all frequencies in NEMOH. The added mass matrix $M_{add}(\omega)$ and radiation damping matrix $B(\omega)$ is calculated for each frequency. The roll equation of motion, after tank is accommodated in platform, is demonstrated in equation 8 and is reiterated as follows:

$$-[M_{44} + M_{add44} + A_{tank44}]\omega^2\varphi - i\omega\ [B_{44} + B_{tank44}]\ \varphi + [K_{44} + K_{tank44}]\varphi = F_E \tag{22}$$

The resultant moment imparted by tank appears as added mass A_{tank44} and damping coefficient B_{tank44} in equation of motion. The formulations to obtain both added mass and damping coefficients from resultant moment of tank is shown in equations 16 and 17, reiterated as follows:

$$A_{44tank} = M_R.\varphi_a.cos\ (\varepsilon) \tag{23}$$

$$B_{44tank} = M_R.\varphi_a.sin\ (\varepsilon) \tag{24}$$

Since both these coefficients depend on frequency, they cannot be directly added into one NEMOH case file with a frequency range. Hence a python-based batch script (shown in Annexure-C) was developed for analysis in NEMOH. This script copies the case folder files according to number of frequencies, sets one frequency in each case folder, adds the damping coefficient B_{44tank} calculated from equation 17 to 44 index in B_{add} matrix, adds added mass coefficient A_{44tank} calculated from equation 16 to 44 index of *Inertia* matrix, and finally runs the solver in each copied folder. The geometry in parent case folder already contains the meshed geometry before copying, so that only the solver and post processing needs to be executed in each copied case directory.

6.6 RAO of Platform Without Tank

The roll RAO provided by FPP are calculated at oirgin of platform with no trim, as discussed previously in section 4.3. To see the effect of tank damping on roll response of platform, the RAO of platform with and without tank needs to be compared. For this purpose, the RAO of platform without any tank installed in platform, needs to be first evaluated in NEMOH and compared with the RAO provided by FPP. The comparison of undamped (without any viscous damping) roll RAO of platform from FPP and the one generated by NEMOH while using mass and stiffness matrices provided by FPP, are shown in Figure 6-3. From the graph, it can be seen that NEMOH results (using FPP matrices) closely align with FPP results. Wave direction of 90 degrees and a water depth of 65 m, corresponding to deep sea conditions were used in the analysis.

Roll RAO of platform with viscous damping, provided by FPP is shown in Figure 6-4. In the graph, the first peak that appears is caused by roll, but the second peak is caused by hydrodynamic coupling. When beam waves strike port or starboard cross-bridge of platform, it is possible that there is a crest on the cross-bridge side while a trough is present at tail-side of platform, creating a pitch motion. The coupling can also be caused by yaw motion. When the beam waves hit the cross-bridge columns before they strike the tail column, the platform undergoes yaw. Therefore, the roll response of platform shows a second peak due to this hydrodynamic coupling effect.

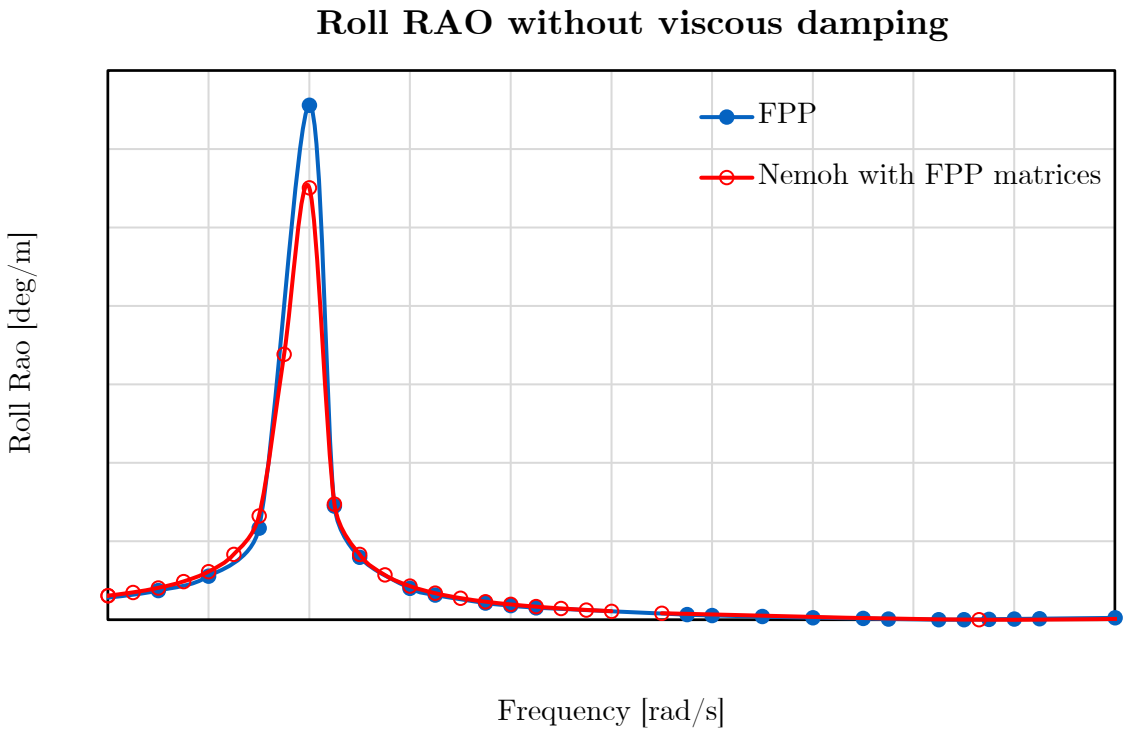

Figure 6-3: Comparison of undamped roll RAO from NEMOH and FPP (without RDT)

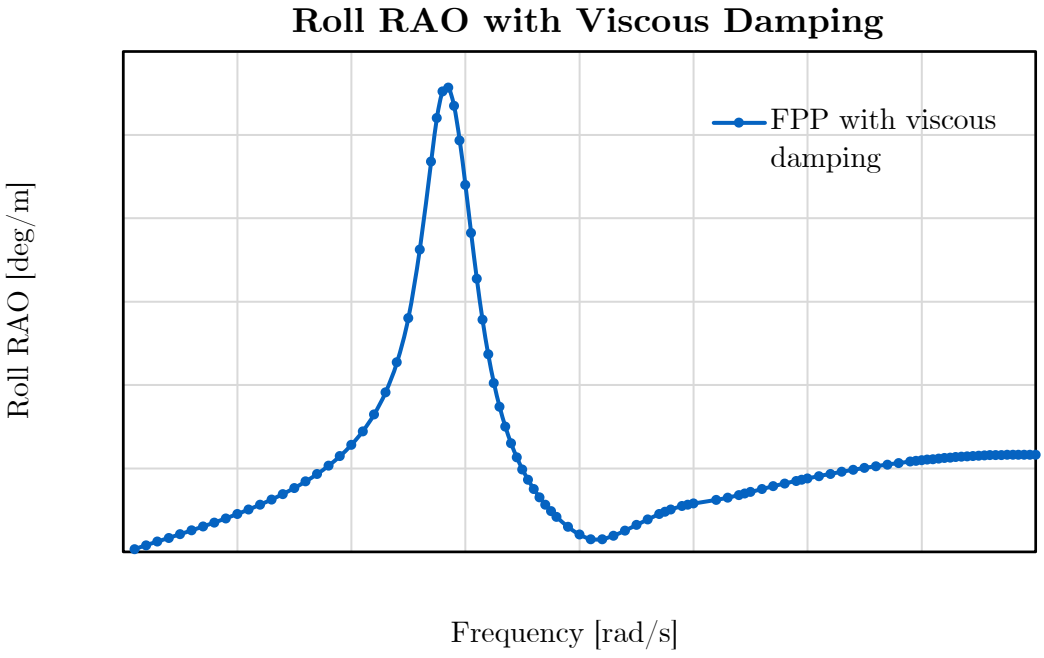

Figure 6-4: Roll RAO from FPP with viscous damping

To match the viscous damping results of FPP, an iterative process of changing roll damping coefficient values (at 44 index) in added damping matrix B_{add} was performed. The fitting of NEMOH results with the FPP viscous damped roll RAO yielded a value of 2.4×10^8 N.m.s for B_{44}. The results of this fitting are shown in Figure 6-5.

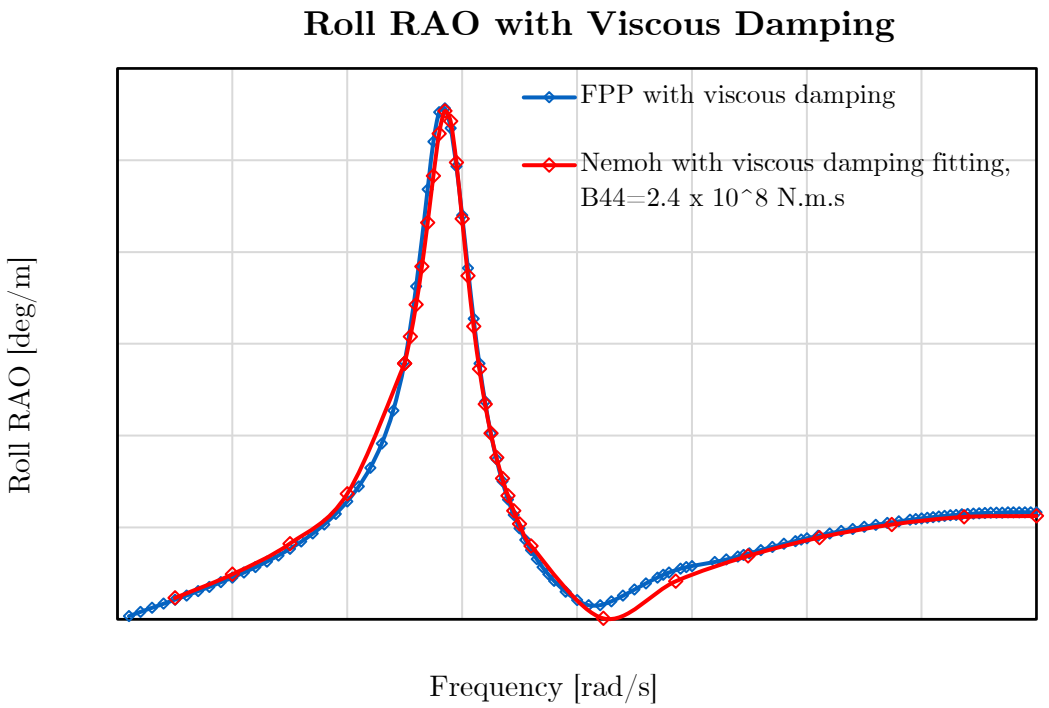

Figure 6-5: NEMOH RAO with viscous damping, fitted with FPP RAO

It can be seen that the second peak of NEMOH fitted curve shows slight difference. It is because only the roll damping coefficient values were changed, and the damping added due to coupling effects was not introduced. Since the focus is on peak resonance frequency values to calculate roll reduction, the slight difference in the second peak can be disregarded.

The viscous damping in FPP platform is linearized from time domain model of platform's motion. Since the platform motion changes once RDT is integrated in platform, the same viscous damping values are no longer applicable. Therefore, the accurate viscous damping values need to be calculated by accommodating tank mass in the time domain model of platform. However, in the present study, the value of viscous damping calculating by fitting NEMOH curve with FPP was selected for further analysis.

6.7 RAO of Platform with Tank

When the tank is integrated into the platform, it is installed in the cross-bridge, which raises the vertical center of gravity. As discussed previously, the displacement of platform will remain same due to ballast compensation. The details of revised mass properties and CoG of platform, in presence of the tank are shown in Table 9-7 in Annexure-C. The change in VCG implies that mass distribution and GM of platform fitted with tank will change, consequently changing the roll stiffness of platform. To investigate the effect of roll damping imparted by tank, the RAO of platform with tank mass and stiffness effect needs to be compared with the RAO that includes tank mass, altered stiffness and added mass & damping coefficients imparted by resultant moment of tank.

6.7.1 Effect of Tank on Platform Stiffness

When tank is integrated in platform, the CoG of platform without trim changes. This leads to a change in transverse GM of platform. The formulation for metacentric height calculation is given as:

$$GM = KB + BM - KG \tag{25}$$

The hydrostatics of platform is calculated from meshMagick while second moment of area of waterplane is calculated from Rhinoceros. The resulting hydrostatics of platform with tank is presented in Table 6-1.

Table 6-1: Hydrostatics of platform with tank

KB (at 14 m draft)	Confidential
I_{xx}	
KG without tank	
KG with tank	
GM_T without tank	
GM_T with tank	
K_{44} without tank	
K_{44} with tank	

The roll stiffness K_{44} is calculated from equation 10. As evident from Table 6-1, the new metacentric height of platform with tank gets reduced from [redacted] m to [redacted] m. This reduction in GM will be reflected as increase in amplitude of roll RAO at constant mesh and frequency step.

6.7.2 Effect of Tank on Mass Matrix of Platform

It was required in the tank design evaluation that the displacement of platform should remain unchanged once the tank is added. As mentioned before, the tank mass is compensated by removal of ballast so that the total mass of platform remains same. However, since ballast is located below CoG of platform while tank is added above CoG, the mass matrix of platform will slightly change, based on the new CoG position. To calculate the new mass matrix at the origin, the distribution of mass within the platform at the new CoG is required. However, due to insufficient data on the individual mass distribution, the mass matrix corresponding to the old CoG was used. This approach is justified by the observation that when the CoG is adjusted in NEMOH and the mass matrix is recalculated at the new CoG (as opposed to the origin point where FPP mass matrices are computed), the percentage difference in the roll-coupled terms of the mass matrix is minimal, as detailed in Table 6-2. The terms not shown in the table are zero in the 4th row and 4th column of the mass matrix. This is because NEMOH calculates a

symmetric mass matrix at the center of gravity, assuming that the mass is uniformly distributed in the submerged portion of the geometry.

From Table 6-2, the percentage difference in mass matrix terms coupled with roll motion is below 20%, except for yaw-roll coupling term M_{64}. For the current analysis, it was assumed that this coupling term does not contribute to significant changes in roll RAO of platform. However, to determine the exact effect of yaw-roll coupled mass moment of inertia, a detailed investigation involving the individual mass distribution in platform needs to be performed.

Table 6-2: Effect of change in VCG on roll-related mass matrix terms

at old CoG		at new CoG		% difference
Mass matrix terms	Mass matrix values [kg.m^2]	Mass matrix terms	Mass matrix values [kg.m^2]	
M_{44}		M_{44}		19.00%
M_{45}		M_{45}		0.00%
M_{46}	Confidential	M_{46}	Confidential	18.21%
M_{54}		M_{54}		20.28%
M_{64}		M_{64}		147.53%

6.7.3 RAO of Un-Stabilized Platform with Tank

The roll RAO of the platform, which includes the tank mass and the altered roll stiffness but excludes the added mass and damping coefficient from the tank moment, is referred to as the un-stabilized RAO of the platform with the tank in this report.

Table 6-3: Effect of tank addition on eigen frequency of platform

	Eigen frequency [rad/s]	
	With viscous damping	Without viscous damping
Platform without tank	Confidential	
Platform with tank		

Once the tank mass and change in roll stiffness due to tank addition is accommodated, the eigen frequency of platform with tank reduces. The effect of tank addition in the un-stabilized roll RAO with and without viscous damping is shown in Figure 6-6 and Figure 6-7. The new eigen frequencies of platform with and without viscous damping are shown in Table 6-3.

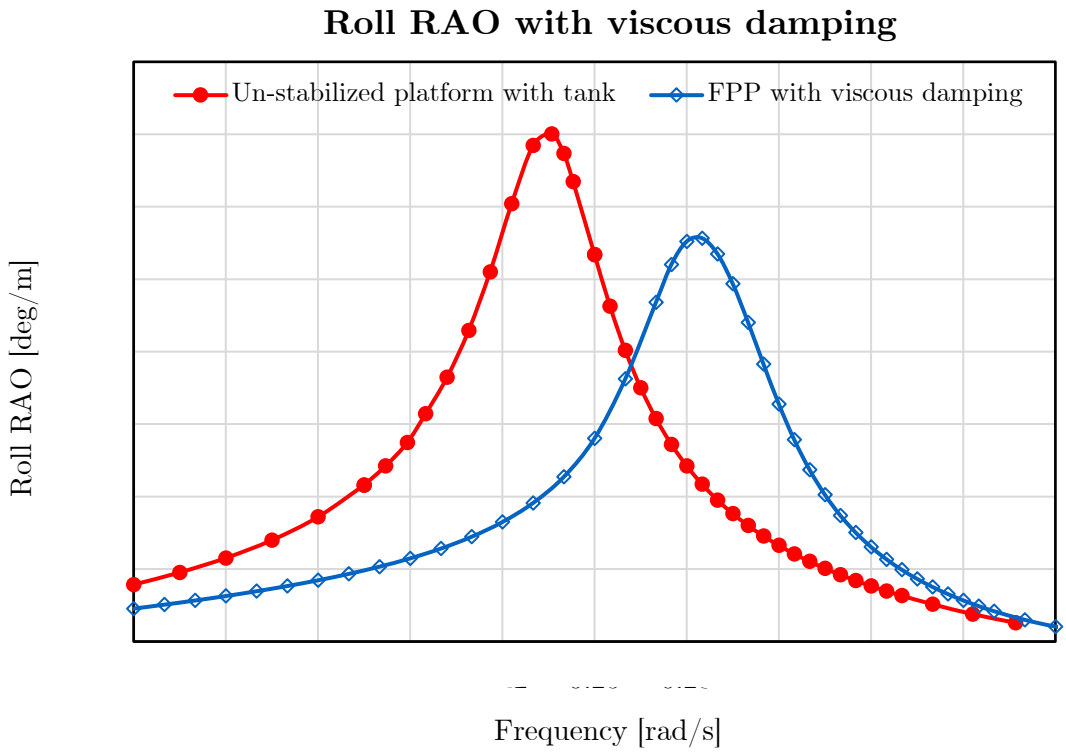

Figure 6-6: Effect of tank addition on roll RAO with viscous damping

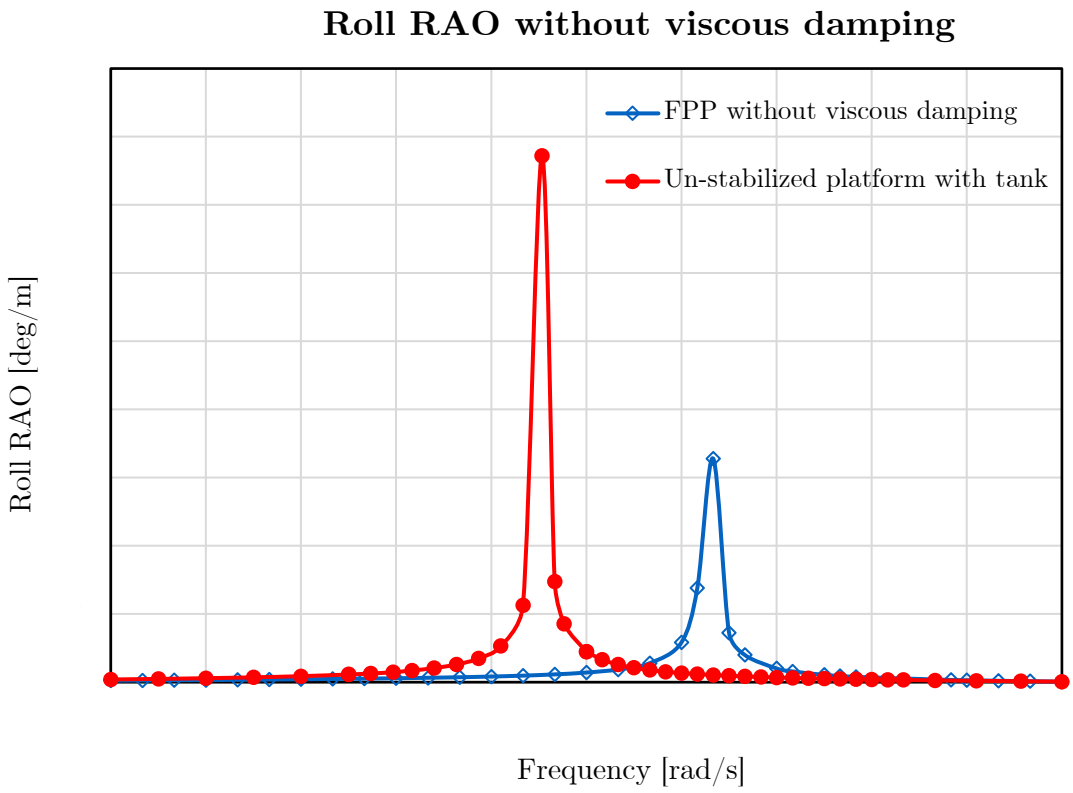

Figure 6-7: Effect of tank addition on roll RAO without viscous damping

6.7.4 RAO of Platform Stabilized by Tank

The effect of tank's resultant moment was applied as added mass and damping coefficient in the motion analysis of platform with tank. The Table 9-8, showing values of these coefficients, obtained from designed tank's resultant moment, is attached in Annexure-C.

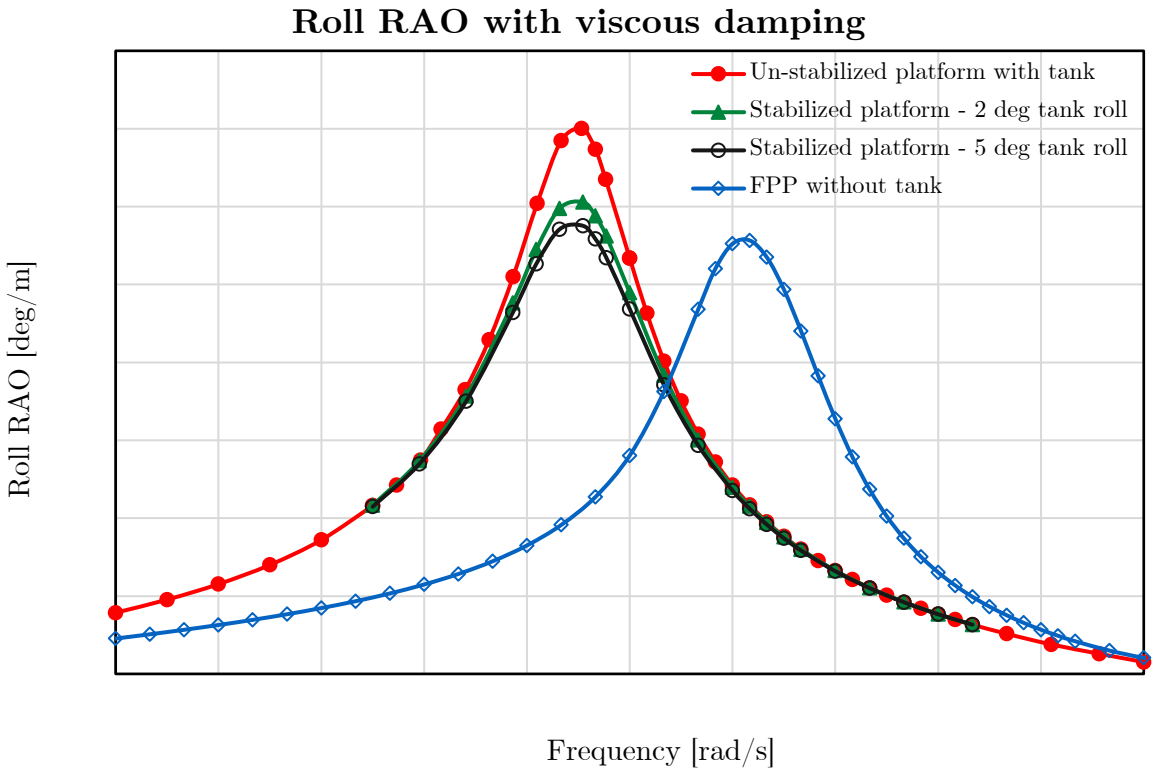

Figure 6-8: Effect of tank damping on roll RAO with viscous damping

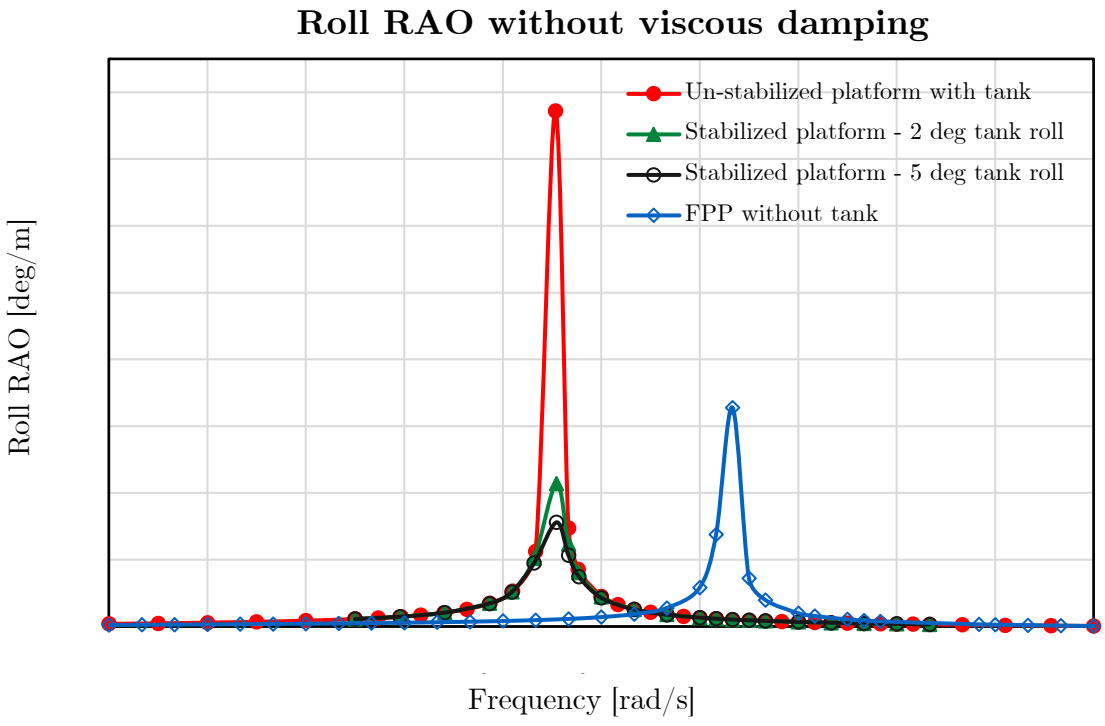

Figure 6-9: Effect of tank damping on roll RAO without viscous damping

The roll RAO of platform stabilized by 2° and 5° roll amplitude tank damping is shown in Figure 6-8 and Figure 6-9. At Hoppe, the roll amplitudes are selected for roll reduction calculation based on the stabilized roll response of vessel, in different wave heights. If the stabilized roll response is below 3.5°, moment-phase curves with 2° roll amplitude are selected for roll reduction calculation. If it is above 3.5° and below 7.5°, then the moment-phase curves at 5° roll amplitude are utilized for roll reduction evaluation. For current analysis, moment-phase curves at 2° and 5° tank roll amplitudes were selected to calculate percentage roll reduction values. The percentage peak roll reduction values are calculated by using both the un-stabilized RAO of platform with tank and FPP RAO without tank. The peak values of RAOs calculated for all case studies are shown in Table 6-4 and the percentage reduction values are presented in Table 6-5.

Table 6-4: Peak values of roll RAO for different case studies

	FPP without tank	Un-stabilized platform with tank	Tank damping at 2° Roll Amp	Tank damping at 5° Roll Amp
Peak RAO [deg/m] with viscous damping	Confidential			
Peak RAO [deg/m] w/o viscous damping	Confidential			

Table 6-5: Percentage roll reduction of platform with RDT damping

	2° Tank Roll Amplitude		5° Tank Roll Amplitude	
Reference Roll RAO	% roll reduction (w/o viscous damping)	% roll reduction (with viscous damping)	% roll reduction (w/o viscous damping)	% roll reduction (with viscous damping)
Un-stabilized platform with tank	72.24%	13.51%	79.79%	17.87%
FPP results	34.67%	-8.84%	52.43%	-3.37%

From Table 6-5 and plots in Figure 6-8 & Figure 6-9, it can be seen that the greatest roll reduction provided by tank occurs when viscous damping is ignored. However, with viscous damping included in the motion analysis, only 13.51% and 17.87% roll reductions for 2° and 5° roll amplitudes, respectively, are observed compared to the un-stabilized RAO of the platform with the tank. In comparison with the original viscous damped RAO from FPP without tank, the designed tank increases the roll motion rather than reducing it. This is because of two factors:

- The peak of roll RAO increases with a decrease in roll stiffness of platform due to elevation in VCG, once the tank is integrated.

- The roll viscous damping value of platform in B_{44} coefficient is on the order of magnitude 10^8. In contrast, the maximum damping coefficient calculated from the designed RDT's moment is on the order of magnitude 10^7. This indicates that viscous damping has a more significant effect in reducing the roll motion of the platform compared to the damping provided by the designed tank.

These reduction values are calculated through sea-keeping analysis in regular waves. In current analysis, the criteria of at least 50% roll reduction compared with RAO provided by FPP is passed by tank with 5° roll amplitude on a platform without viscous damping. In comparison with the RAO modified by tank addition, the criterion is passed by both 2° and 5° tank roll amplitudes in analysis without viscous damping.

7 CONCLUSIONS

In this thesis, the effect of Roll Damping Tank (RDT) on the motion of a semi-submersible Floating Offshore Wind Turbine (FOWT) platform was investigated. For this purpose, a T-shaped semi-submersible platform, "SEAWORTHY", designed by Floating Power Plants (FPP) was selected. A C-shaped box tank was designed in such a way that the tank dimensions and water-level lead to a tank roll period that closely matches the eigen roll period of platform.

After preliminary design evaluation of tank, a parametrized model of tank was developed, and the resultant moment-phase diagram of designed tank was calculated via k-epsilon turbulence modelling in OpenFOAM. To validate OpenFOAM results, two benchmark studies on tanks already tested at Hoppe i.e. Field & Martin tank and HERMes tank were conducted. Convergence study was performed at the resonance frequency for Field & Martin tank; however, for HERMes tank, only two meshes were assessed due to increase in computational time with the mesh refinement. For both tanks, it was observed that interFoam solver with k-epsilon turbulence modelling gives the closest results while interIsoFoam causes peak shift. The comparison of previous Bench Model Tests (BMTs) and the CFD study on Field & Martin tank indicated a lack of consistency in prior results. Consequently, Field & Martin cannot be relied upon for the validation of CFD results. The HERMes tank CFD results demonstrated close agreement with resultant moment-phase diagrams at 5° and 10° roll amplitudes. However, the 2° resultant moment curve of the OpenFOAM results showed a constant positive offset from the BMT moment diagram, indicating that the BMT results were consistently lower than the OpenFOAM results at all frequencies. For phase diagram, there was close conformity for all roll amplitudes, except for some deviations at higher frequencies. To investigate this offset and discrepancies at higher frequency, another turbulence model i.e. k-omega SST and a refined mesh were analysed. It was found that while k-omega SST leads to higher offsets at 2° roll amplitude, the refined mesh leads to a decrease in offset and lower discrepancies in moment-phase diagram at higher frequencies. The resultant moment of tank, obtained from CFD analysis, was applied as added mass and damping coefficient in the motion analysis of platform.

Afterwards, sea-keeping analysis of platform was performed in NEMOH and the roll RAOs of platform, with and without tank were investigated. A mesh convergence study for number of panels was performed beforehand and roll RAO of different panels around peak frequency were compared. It was found that the results largely depend on number of panels in transverse surfaces of platform columns. To validate sea-keeping results in NEMOH, the roll RAOs of platform with and without viscous damping, provided by FPP, were compared with roll RAO of platform obtained in NEMOH. It was observed that RAO of platform calculated by NEMOH, without incorporating the viscous damping, closely matched with the undamped roll RAO provided by FPP. Roll RAO with viscous damping, provided by FPP, incorporated drag linearized from time domain model of platform's motion. The RAO produced by NEMOH was fitted with the viscous damped RAO from FPP, by changing the added damping matrix at B_{44} index. This led to an RAO in NEMOH that coincided with the first peak of RAO from FPP; however, the second peak showed some variations. It was determined that the second peak

arises from hydrodynamic coupling. Consequently, an added damping value at the B_{45} index is necessary to achieve perfect agreement between the NEMOH and FPP plots with viscous damping.

Since the platform motion changes once RDT is integrated in platform, the effect of tank addition on mass matrix and roll stiffness of the platform was evaluated. It was observed that tank addition increases the peak of roll response while decreasing the platform's eigenfrequency. The roll reduction values for the stabilized platform were calculated for both cases: with viscous damping and without viscous damping. For roll reduction evaluation, both the FPP RAO without tank and the modified RAO of un-stabilized platform after tank addition were used as a reference.

Following observations and conclusions were drawn from the overall analysis performed in this thesis:

- The design of tank was limited by the total ballast available for compensation of added tank mass. It was also limited by the space available in General Arrangement (GA) of platform. These factors constrain the design of a tank capable of providing the maximum damping moment while ensuring the roll period aligns with the eigen period of the platform.
- A methodology was successfully developed that enables the parametrization of tank geometry and automates the computation of RDT across different roll amplitudes and frequency combinations, all utilizing open-source tools.
- CFD analysis of tank via k-epsilon turbulence modelling in OpenFOAM can provide moment-phase diagrams that closely resemble the ones obtained through Bench Model Tests (BMTs). The agreement of CFD results with BMT improved with mesh refinement.
- NEMOH can be used to apply added mass and damping coefficient, imparted by tank moment in calculation of roll RAO. To achieve this, each frequency needs to be separately analysed and tank coefficients need to be added via a batch script. However, sea-keeping analysis in NEMOH is limited to regular waves only and can only provide a rough estimate of roll reduction.
- It was required that the integrated RDT should not change the draft or displacement of platform. To meet this requirement, ballast at the bottom of the platform column was replaced by tank mass in the cross-bridge. This moves the VCG of platform upwards, thereby reducing the transversal metacentric height and changing eigen frequency of platform.
- Decrease in metacentric height and consequently roll stiffness of platform, due to tank addition, leads to a decrease in eigen frequency of platform and an increase in roll RAO peak (shown in Figure 6-6 and Figure 6-7). This necessitates that the RAO with tank damping should be compared not only with the original FPP RAO without tank, but also with the un-stabilized RAO of platform with tank.
- The maximum roll reduction with viscous damping, 17.87%, is achieved by the tank at a 5° roll amplitude, using the un-stabilized platform with tank as a reference (see Figure 6-8 and Table 6-5). For case studies with the effect of viscous damping included, it was

observed that the designed tank increases the roll motion rather than reducing it, when compared with FPP RAO of platform without tank.

- In the absence of viscous damping, the maximum roll reduction was calculated to be 79.8% using the un-stabilized platform with tank as a reference, and 52.43% using the FPP RAO without tank as a reference (see Figure 6-9 and Table 6-5).
- It was found that the viscous damped platform from FPP already has high initial damping, which reduces the efficacy of RDT in damping the roll motion. The roll damping coefficient values differed from roll viscous damping value by the order of 10, which indicated that viscous damping was more significant than tank damping for the given platform. In other words, regardless of the tank design's quality, the platform's high initial viscous damping will significantly limit the tank's roll damping effectiveness in regular waves.
- The location available for tank integration in platform increases the VCG, leading to increase in roll RAO. For efficient tank design, the tank should be integrated in such a location which does not change the VCG of platform.

7.1 Future Recommendations

To further validate the results obtained in this study, following recommendations are suggested:

- CFD analysis of HERMes tank should be performed with finer meshes to investigate the reason of offset in resultant moment diagram at 2° roll amplitude.
- Investigation on change in mass distribution of platform and its effect on roll RAO, when the total displacement of platform remains same, should be further pursued.
- The viscous damping values of platform with tank integration need to be investigated. This is essential to obtain realistic roll reduction values.
- Only regular waves were considered in the current analysis, and the non-linear changes in RAO with wave amplitude were not addressed by NEMOH. Future sea-keeping studies should examine the impact of tank damping in irregular waves to provide a more comprehensive understanding.

8 REFERENCES

[1] T. Perez and M. Blanke, "Ship roll damping control," *Annu Rev Control*, vol. 36, no. 1, pp. 129–147, 2012, doi: 10.1016/j.arcontrol.2012.03.010.

[2] N. Alujević, I. Ćatipović, Malenica, I. Senjanović, and N. Vladimir, "Stability, performance and power flow of active U-tube anti-roll tank," *Eng Struct*, vol. 211, May 2020, doi: 10.1016/j.engstruct.2020.110267.

[3] Tanumoy Sinha, "Different Types Of Roll Stabilization Systems Used For Ships." Accessed: Jul. 27, 2024. [Online]. Available: https://www.marineinsight.com/naval-architecture/roll-stabilization-systems/

[4] X. Mei and M. Xiong, "Effects of second-order hydrodynamics on the dynamic responses and fatigue damage of a 15 mw floating offshore wind turbine," *J Mar Sci Eng*, vol. 9, no. 11, Nov. 2021, doi: 10.3390/jmse9111232.

[5] E. C. Edwards, A. Holcombe, S. Brown, E. Ransley, M. Hann, and D. Greaves, "Evolution of floating offshore wind platforms: A review of at-sea devices," Sep. 01, 2023, *Elsevier Ltd.* doi: 10.1016/j.rser.2023.113416.

[6] H. M. Johlas, L. A. Martínez-Tossas, M. J. Churchfield, M. A. Lackner, and D. P. Schmidt, "Floating platform effects on power generation in spar and semisubmersible wind turbines," *Wind Energy*, vol. 24, no. 8, pp. 901–916, Aug. 2021, doi: 10.1002/we.2608.

[7] Y. Liu, Q. Xiao, A. Incecik, and D. C. Wan, "Investigation of the effects of platform motion on the aerodynamics of a floating offshore wind turbine," *Journal of Hydrodynamics*, vol. 28, no. 1, pp. 95–101, Feb. 2016, doi: 10.1016/S1001-6058(16)60611-X.

[8] T. Chatterjee and S. Chakraborty, "Vibration mitigation of structures subjected to random wave forces by liquid column dampers," *Ocean Engineering*, vol. 87, pp. 151–161, Sep. 2014, doi: 10.1016/j.oceaneng.2014.05.004.

[9] R. Sardar and S. Chakraborty, "Wave induced vibration control of offshore jacket platform by tuned liquid damper with floating base," *Ocean Engineering*, vol. 273, Apr. 2023, doi: 10.1016/j.oceaneng.2023.113948.

[10] J. Vasta, "Roll stabilization by means of passive tanks," *Trans SNAME*, 1961.

[11] C. Stigter, "The performance of U-tanks as a passive anti-rolling device," *International Shipbuilding Progress*, vol. 13, no. 144, pp. 249–275, Aug. 1966, doi: 10.3233/ISP-1966-1314401.

[12] J. W. W. P. Bell, "Activated and passive controlled fluid tank system for ship stabilization," 1966.

[13] W. W. C., "Analysis of the control of activated antiroll tanks.," *Trans SNAME*, vol. 76, pp. 296–331, 1968, Accessed: Jul. 30, 2024. [Online]. Available: https://cir.nii.ac.jp/crid/1571417124093993344

[14] S. B. Field and J. P. Martin, "COMPARATIVE EFFECTS OF U-TUBE AND FREE SURFACE TYPE PASSIVE ROLL STABILISATION SYSTEMS.," *Naval Architect*, no. 2, pp. 73–92, 1976.

[15] G. Lewison, "Optimum design of passive roll stabilizer tanks," *Naval Architect*, 1976.

[16] R. A. Barr and V. Ankudinov, "Ship Rolling, Its Prediction and Reduction Using Roll Stabilization," *Marine Technology and SNAME News*, vol. 14, no. 01, pp. 19–41, Jan. 1977, doi: 10.5957/mt1.1977.14.1.19.

[17] W. and D. J. and B. R. Webster, "Prediction and measurement of the performance of free-flooding ship antirolling tanks," *Society of Naval Architects and Marine Engineers-Transactions*, 1988.

[18] B. S. Lee and D. Vassalos, "An investiation into the stabilisation effects of anti-roll tanks with flow obstructions," *International Shipbuilding Progress*, vol. 43, no. 433, pp. 70–88, 1996.

[19] A. F. A. Gawad, S. A. Ragab, A. H. Nayfeh, and D. T. Mook, "Roll stabilization by anti-roll passive tanks," 2001.

[20] M. Borg, E. U. Ortigado, M. Collu, and F. P. Brennan, "Passive damping systems for floating vertical axis wind turbines analysis."

[21] Marea Anna Franzel, "Design and Feasibility Study of an Anti-Roll Tank for Floating Offshore Wind Turbine Foundation," École Centrale de Nantes, 2019.

[22] Fukushima Offshore Wind Consortium, "Fukushima Floating Offshore Wind Farm Demonstration Project (Fukushima FORWARD)--Construction of Phase II." [Online]. Available: http://www.fukushima-forward.jp

[23] Principle Power, "Projects: WindFloat Atlantic." Accessed: Jul. 03, 2024. [Online]. Available: https://www.principlepower.com/projects/windfloat-atlantic

[24] Advanced Structures & Composites Center - University of Maine, "VolturnUS," *https://composites.umaine.edu/*, Accessed: Jul. 03, 2024. [Online]. Available: https://composites.umaine.edu/offshorewind/volturnus/

[25] Power Technology, "Groix & Belle-Ile Floating Offshore Wind Farm." Accessed: Jul. 03, 2024. [Online]. Available: https://www.power-technology.com/projects/groix-belle-ile/

[26] Floating Power Plant, "Welcome to SEAWORTHY: Revolutionizing Offshore Power with Clean Energy." Accessed: Jul. 03, 2024. [Online]. Available: https://floatingpowerplant.com/commercial-demonstrator-project/

[27] Bassoe Technology, "Bassoe Technology Floater Design ", Accessed: Jul. 03, 2024. [Online]. Available: https://www.basstech.se/17/11/renewables/

[28] T. Hendriks and J. Mendonca Santos, "Challenges in stability of offshore floating structures," 2017, p. 13.

[29] I. J. Hsu *et al.*, "Optimization of Semi-submersible Hull Design for Floating Offshore Wind Turbines," in *Proceedings of the International Conference on Offshore Mechanics and Arctic Engineering - OMAE*, American Society of Mechanical Engineers (ASME), 2022. doi: 10.1115/OMAE2022-86751.

[30] OpenFast, "OpenFAST Documentation: SubDyn User Guide and Theory Manual." Accessed: Jul. 04, 2024. [Online]. Available: https://openfast.readthedocs.io/en/dev/source/user/subdyn/input_files.html

[31] A. H. Techet, "2.016 Hydrodynamics." Accessed: Aug. 03, 2024. [Online]. Available: https://web.mit.edu/2.016/www/handouts/2005Reading6.pdf

[32] M. K. Al-Solihat and M. Nahon, "Mooring and hydrostatic restoring of offshore floating wind turbine platforms," in *2014 Oceans - St. John's, OCEANS 2014*, Jul. 2015. doi: 10.1109/OCEANS.2014.7003269.

[33] Massachusetts Institute of Technology, "WAMIT USER MANUAL," 2023. [Online]. Available: www.wamit.com

[34] MathWorks, "filtfilt." Accessed: Jul. 29, 2024. [Online]. Available: https://de.mathworks.com/help/signal/ref/filtfilt.html

[35] OpenFoam Wiki, "InterFoam." Accessed: Jul. 10, 2024. [Online]. Available: https://openfoamwiki.net/index.php/InterFoam

[36] SimFlow, "interIsoFoam - OpenFOAM Solver." Accessed: Jul. 10, 2024. [Online]. Available: https://help.sim-flow.com/solvers/inter-iso-foam

[37] SimFlow, "Courant Number in CFD." Accessed: Jul. 10, 2024. [Online]. Available: https://sim-flow.com/courant-number-in-cfd/

[38] WolfDynamics, "Dynamic meshes in OpenFOAM," 2014.

[39] S. B. Field and J. P. Martin, "Comparative effects of U-tube and free surface type passive roll stabilisation systems," *Trans RINA*, vol. 118, pp. 73–92, 1976, Accessed: Jul. 09, 2024. [Online]. Available: https://cir.nii.ac.jp/crid/1573387451276761728

[40] M. Kerkvliet, N. Carette, G. Vaz, and M. Gunsing, "Analysis of U-type anti-roll tank using urans. Sensitivity and validation," *Proceedings of the International Conference on Offshore Mechanics and Arctic Engineering - OMAE*, vol. 2, 2014, doi: 10.1115/OMAE2014-23483.

[41] B. van Leer, "Towards the ultimate conservative difference scheme. II. Monotonicity and conservation combined in a second-order scheme," *J Comput Phys*, vol. 14, no. 4, pp. 361–370, Mar. 1974, doi: 10.1016/0021-9991(74)90019-9.

[42] C. Geuzaine and J.-F. Remacle, "Gmsh: a three-dimensional finite element mesh generator with built-in pre- and post-processing facilities," 2008, [Online]. Available: https://orbi.uliege.be/handle/2268/38595

[43] H. Söding, "Boundary Element Methods for Seakeeping Contribution to the Lectures Boundary Element Methods for Seakeeping," 2010. [Online]. Available: https://www.researchgate.net/publication/260433070

[44] "Amelioration des perfomances des codes de calcul de diffraction radiation au premier ordre | TU Delft Repository." Accessed: Jul. 24, 2024. [Online]. Available: https://repository.tudelft.nl/record/uuid:ee2266b1-f98d-468a-9afc-accead8aa251#files

[45] Ecole Centrale de Nantes, "Nemoh Input/Output." Accessed: Jul. 17, 2024. [Online]. Available: https://lheea.gitlab.io/Nemoh/input-output.html

9 ANNEXURE

Annexure-A

The location of reference point at origin is shown in the following figure.

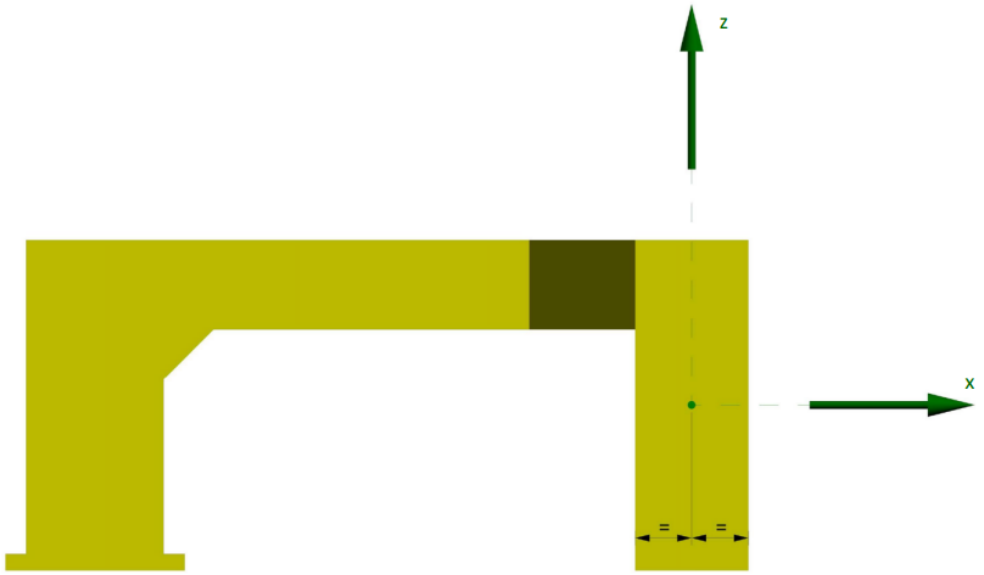

Figure 9-1: Side view of platform showing vertical position of origin

The mass properties of platform from origin are given as:

Table 9-1: Mass properties of platform without tank

	Mass	CoG_x	CoG_y	CoG_z	1st moment_x	1st moment_y	1st moment_z
	[Te]	[mm]	[mm]	[mm]	[Te*mm]	[Te*mm]	[Te*mm]
Aft ballast tank							
STBD ballast tank							
PORT ballast tank				Confidential			
Total weight without ballast							
Total							

The hydrostatics of platform are given as:

Table 9-2: Center of buoyancy of platform

	X [mm]	Y [mm]	Z [mm]
Center of buoyancy		Confidential	

Annexure-B

The dimensions for original Field & Martin tank and its scaled values at 14.5 scale (with tolerances) used at Hoppe is given as:

Table 9-3: Field & Martin tank dimensions (real and model scale)

Quantity		Symbol	Real tank value [m]	Scaled value [m]
Total width	(y-direction)	WT	12.800	0.870
Total length	(x-direction)	LT	5.334	0.360
Wing tank	Width	WW	2.743	
Wing tank	Height	HW	3.048	0.210
Duct width		WD	7.315	0.5
Duct height		HD	0.610	0.044
CoR	above bottom tank	HCR	1.372	0.095
Water filling height		HF	1.525	0.105

The details for Hermes tank dimensions are given as:

Table 9-4: HERMes tank dimensions (real and model scale)

Model Scale		1/26	
		Real Scale(m)	Model Scale(mm)
Length of the tank		9	346.15
Breadth of the tank		48.2	1853.85
Height of the tank		8	307.69
COG to COR		9.7	0.7865
Water Height	Wh1	5.48	210.77
	Wh2	4.65	178.85
	Wh3	3.35	128.85
	Wh4	2.52	96.92

The table showing percentage difference between OpenFOAM results and BMT results of HERMes at 2° amplitude is given as:

Table 9-5: Percentage difference between OpenFOAM and BMT results for HERMes

Resultant Moment [KN.m/deg] at 2° amplitude							
Freq [rad/s]	BMT	0.0154 mesh k-epsilon	%age diff	0.0103 mesh k-epsilon	%age diff	0.0154 mesh k-omega	%age diff
0.07	15031.47	15361.57	2.20%	15239.72	1.39%	15349.31	2.11%
0.16	20648.62	22467.85	8.81%	22158.73	7.31%	22399.73	8.48%
0.18	23777.24	25963.73	9.20%	25511.80	7.30%	25948.23	9.13%
0.21	25790.69	27812.71	7.84%	27204.14	5.48%	28070.10	8.84%
0.24	26103.67	28144.94	7.82%	27419.81	5.04%	28600.13	9.56%
0.27	25807.28	27545.12	6.73%	26817.69	3.92%	28091.04	8.85%
0.30	24737.58	26579.79	7.45%	25667.41	3.76%	27059.21	9.39%
0.32	23004.52	24891.72	8.20%	23911.46	3.94%	25673.80	11.60%
0.35	19786.96	21718.25	9.76%	20839.98	5.32%	22889.68	15.68%
0.38	16593.79	18530.97	11.67%	17783.01	7.17%	19662.92	18.50%
0.41	13180.95	15239.11	15.61%	14934.41	13.30%	16057.35	21.82%
0.43	10817.08	12573.09	16.23%	12393.20	14.57%	13042.40	20.57%
0.46	9170.49	10918.47	19.06%	10666.47	16.31%	11079.22	20.81%
0.49	8037.11	9668.65	20.30%	9406.60	17.04%	9813.48	22.10%
0.52	7319.88	8653.76	18.22%	8428.02	15.14%	8713.05	19.03%
0.54	6806.93	7873.52	15.67%	7736.98	13.66%	7891.37	15.93%
0.57	6584.43	7166.94	8.85%	7055.60	7.16%	7154.69	8.66%
0.60	6393.77	6820.74	6.68%	6645.34	3.93%	6863.52	7.35%
0.63	6237.94	5813.55	-6.80%	5742.11	-7.95%	5860.60	-6.05%

Mass properties for designed tank of FPP platform are given as follows:

Table 9-6: Mass properties for designed platform tank

	Water Level	
	4.6 m	2.8 m
Mass	1115716.053 kg	680 kg
Ixx	269240962.334 kg m^2	163131967.184 kg
VCG	2.3 m	1.4 m
Lever	2.73 m	0.66 m

Annexure-C

Mesh convergence for platform shows that roll RAO peak depends on number of panels on the transverse surface of platform columns.

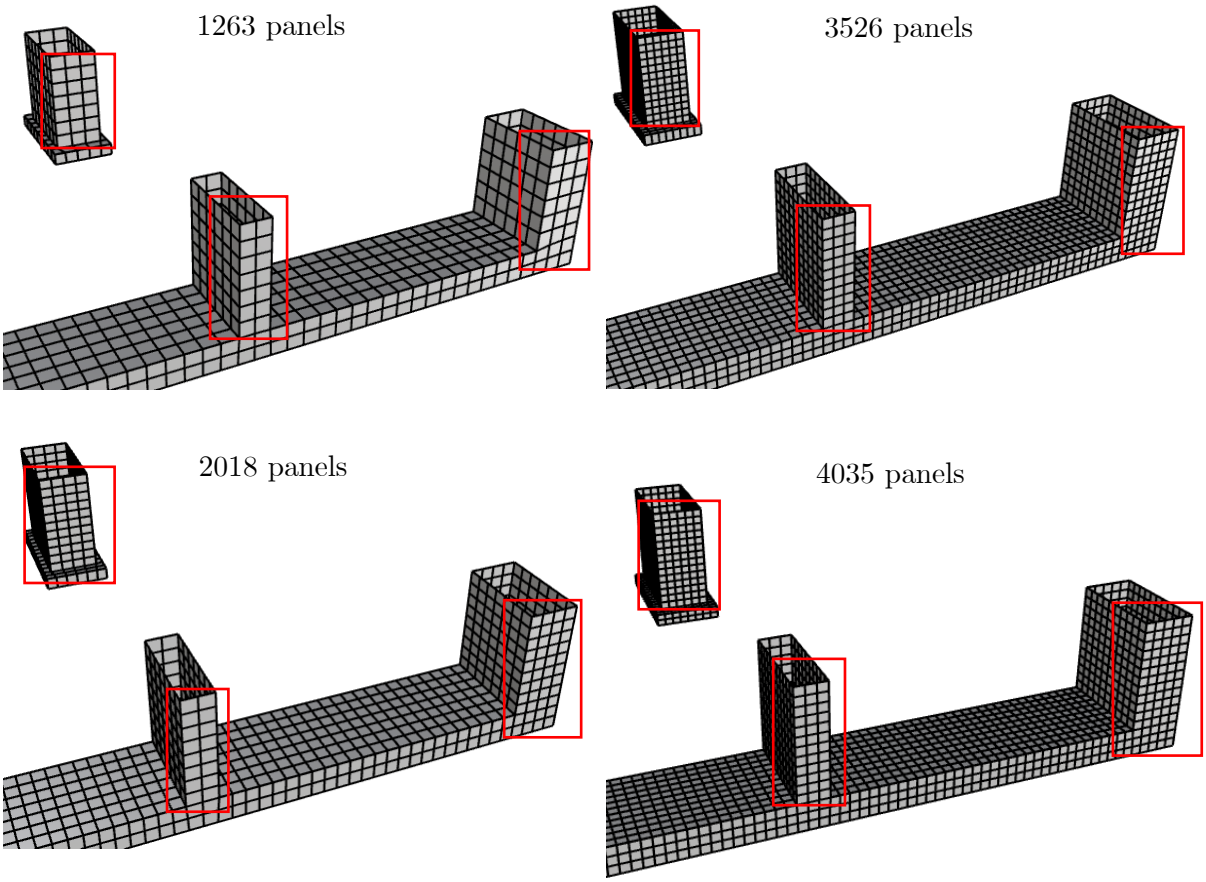

Figure 9-2: Mesh convergence study for platform panels

Table 9-7: Revised mass properties of platform with RDT (from origin)

	Mass [Te]	CoG_x [mm]	CoG_y [mm]	CoG_z [mm]
Aft ballast tank				
Roll damping tank				
STBD ballast tank				
PORT ballast tank			Confidential	
Platform weight				
with WTG				
Total				

The values of added mass and damping coefficients, calculated from resultant moment-phase curve of designed platform tank are shown in the following table:

Table 9-8: Added mass and damping coefficients of designed RDT at 2° roll amplitude

Frequency [rad/s]	M44	B44
[redacted]	3.47E+07	1.27E+07
[redacted]	3.40E+07	2.32E+07
[redacted]	2.65E+07	3.35E+07
[redacted]	1.51E+07	3.87E+07
[redacted]	9.71E+06	3.91E+07
[redacted]	4.86E+06	3.86E+07
[redacted]	1.16E+06	3.76E+07
[redacted]	-2.61E+06	3.59E+07
[redacted]	-5.79E+06	3.39E+07
[redacted]	-9.67E+06	3.06E+07
[redacted]	-1.22E+07	2.69E+07
[redacted]	-1.38E+07	2.32E+07
[redacted]	-1.42E+07	2.16E+07
[redacted]	-1.45E+07	2.02E+07
[redacted]	-1.47E+07	1.87E+07
[redacted]	-1.44E+07	1.76E+07
[redacted]	-1.40E+07	1.55E+07
[redacted]	-1.35E+07	1.37E+07
[redacted]	-1.37E+07	1.14E+07
[redacted]	-1.33E+07	9.31E+06
[redacted]	-1.22E+07	8.22E+06